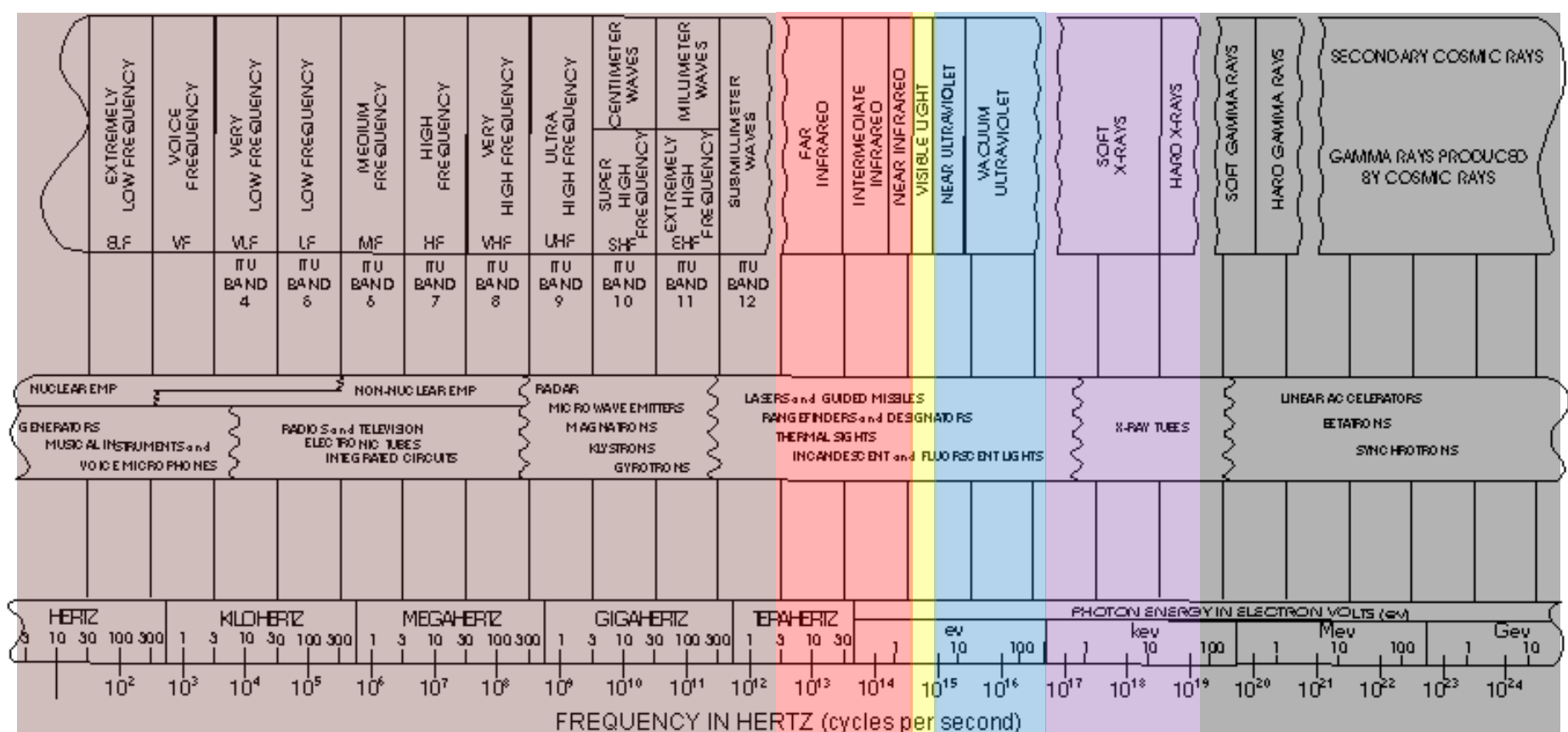


ESTRUCTURA GALÁCTICA Y DINÁMICA ESTELAR

Componentes de la Vía-Láctea

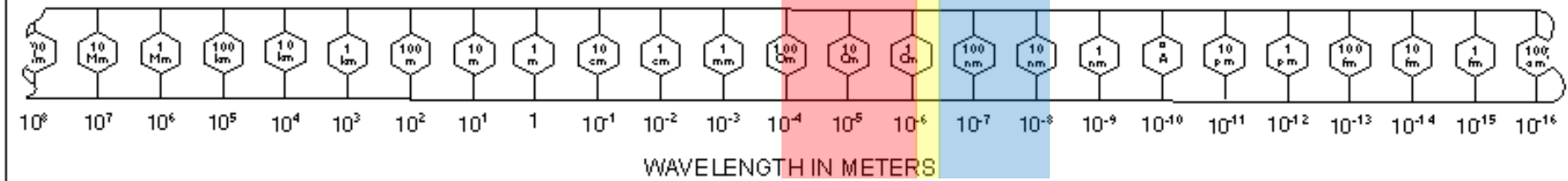


*Componentes de la
Vía-Láctea*



$$1 \text{ Hz} = \text{onda/s}$$

$$1 \text{ eV} = 1.602 \times 10^{-19} \text{ J}$$



electromagnetic spectrum

$$c = \lambda \cdot v$$

$$1 \mu\text{m} = 10^{-6} \text{ m} \quad 1 \text{ \AA} = 10^{-10} \text{ m}$$

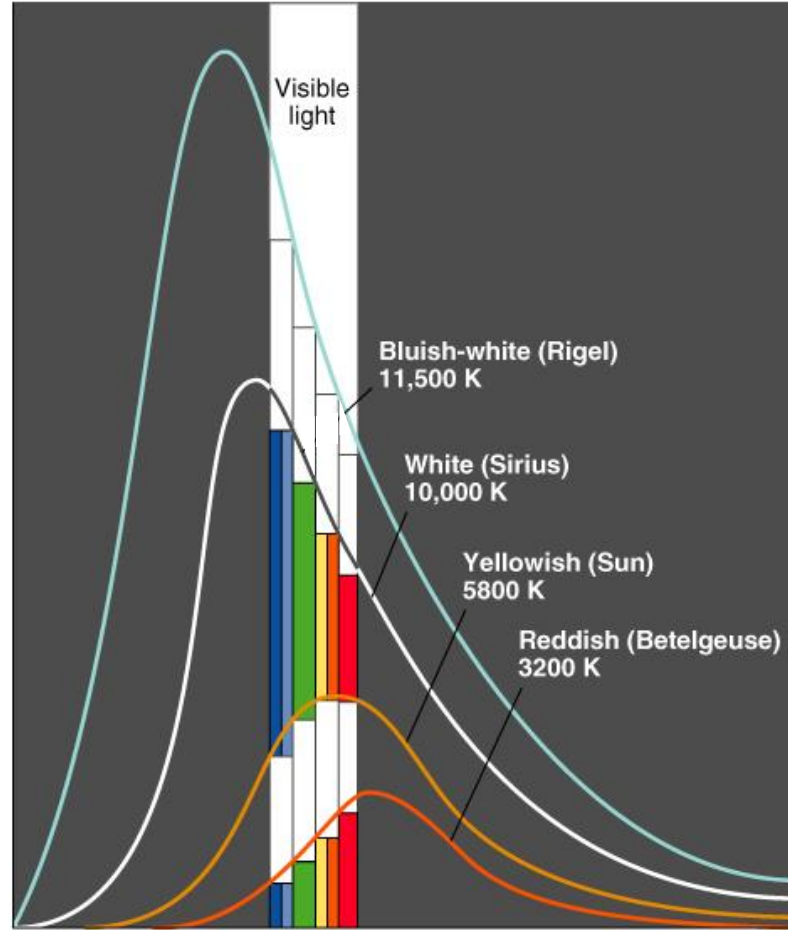
$$E = h \nu = h c / \lambda$$

La Vía-Láctea en óptico/visible (cameras, 3000-7000 Å)

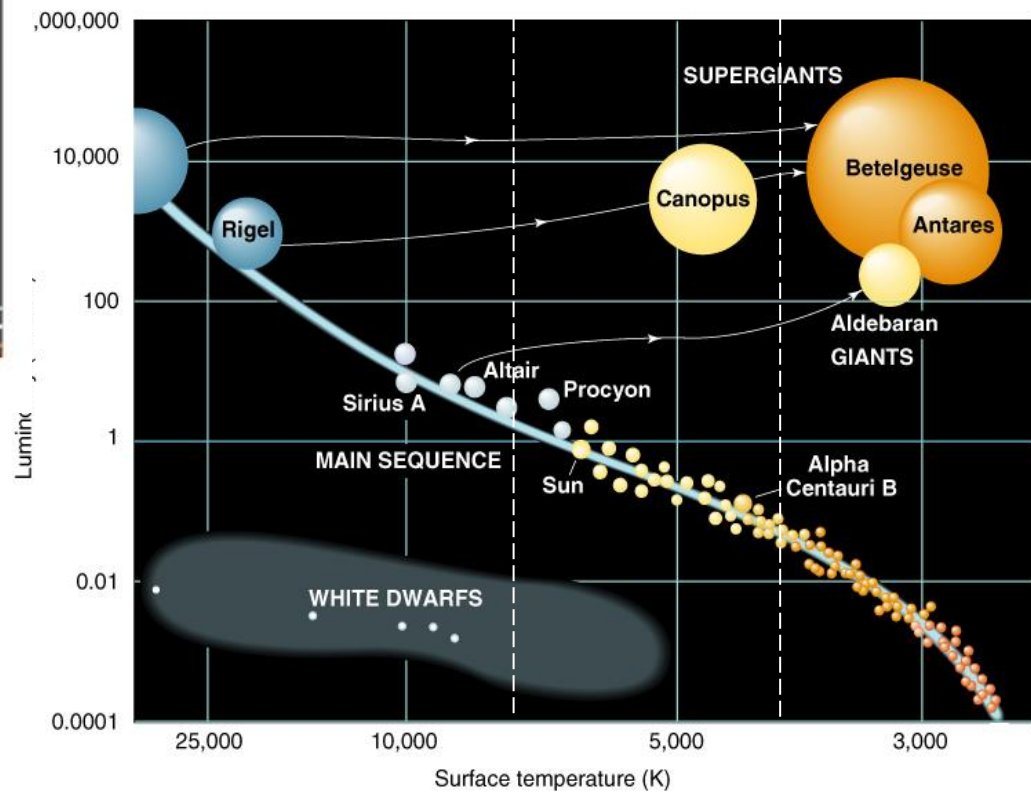


estrellas de temperatura intermedia (Seq. Principal), nubes moleculares (oscuras por el polvo)

Increasing flux

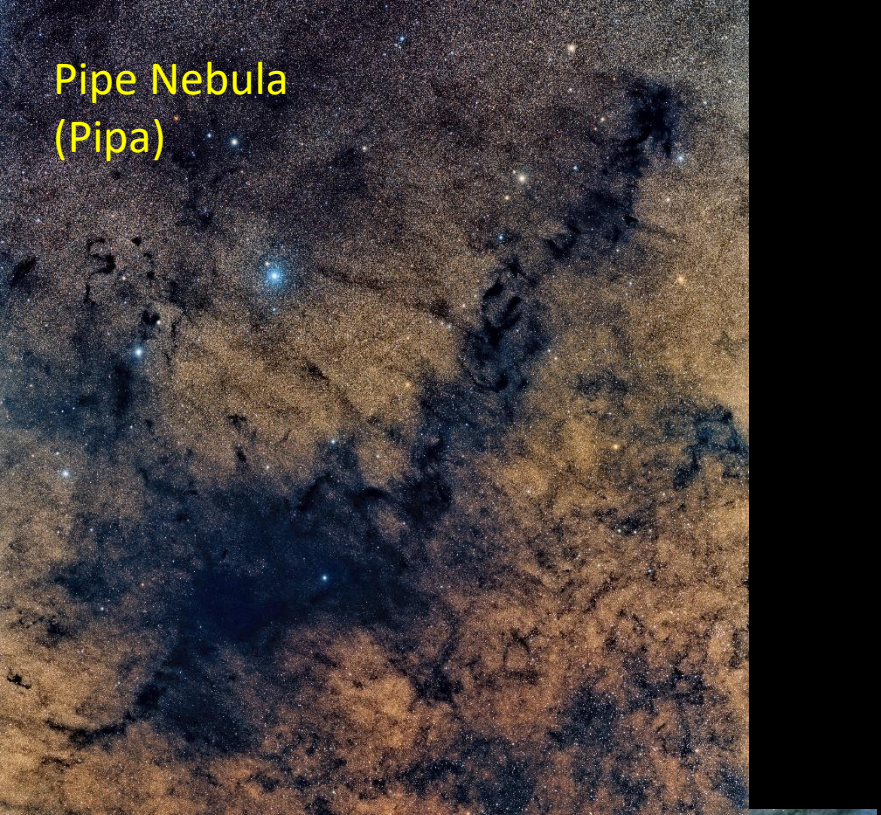


Copyright 1999 John Wiley and Sons, Inc. All rights reserved.

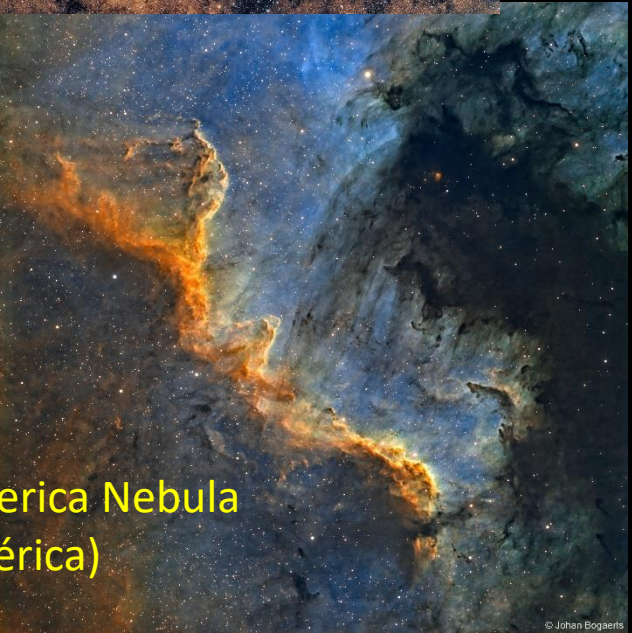


Copyright 1999 John Wiley and Sons, Inc. All rights reserved.

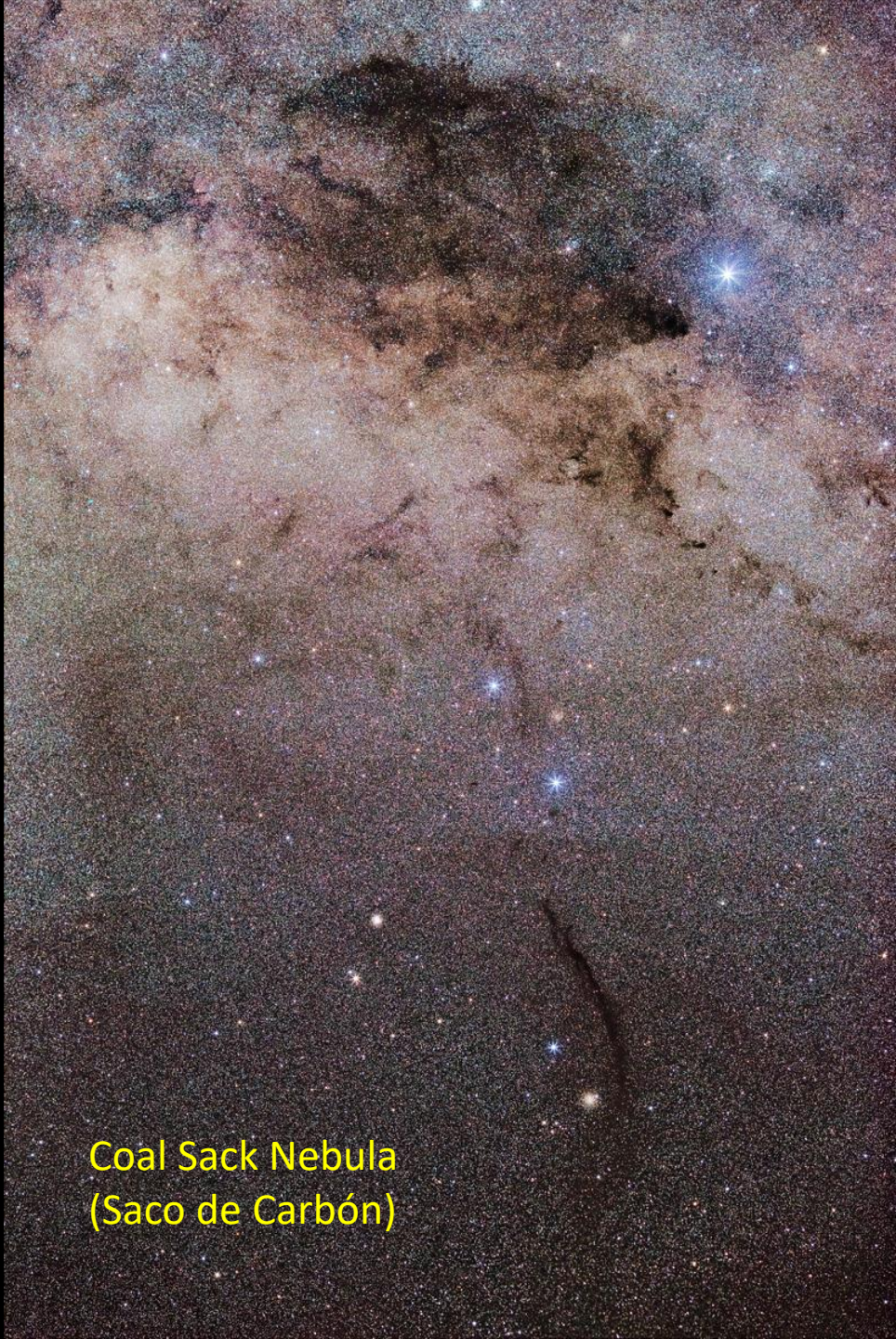
Pipe Nebula
(Pipa)



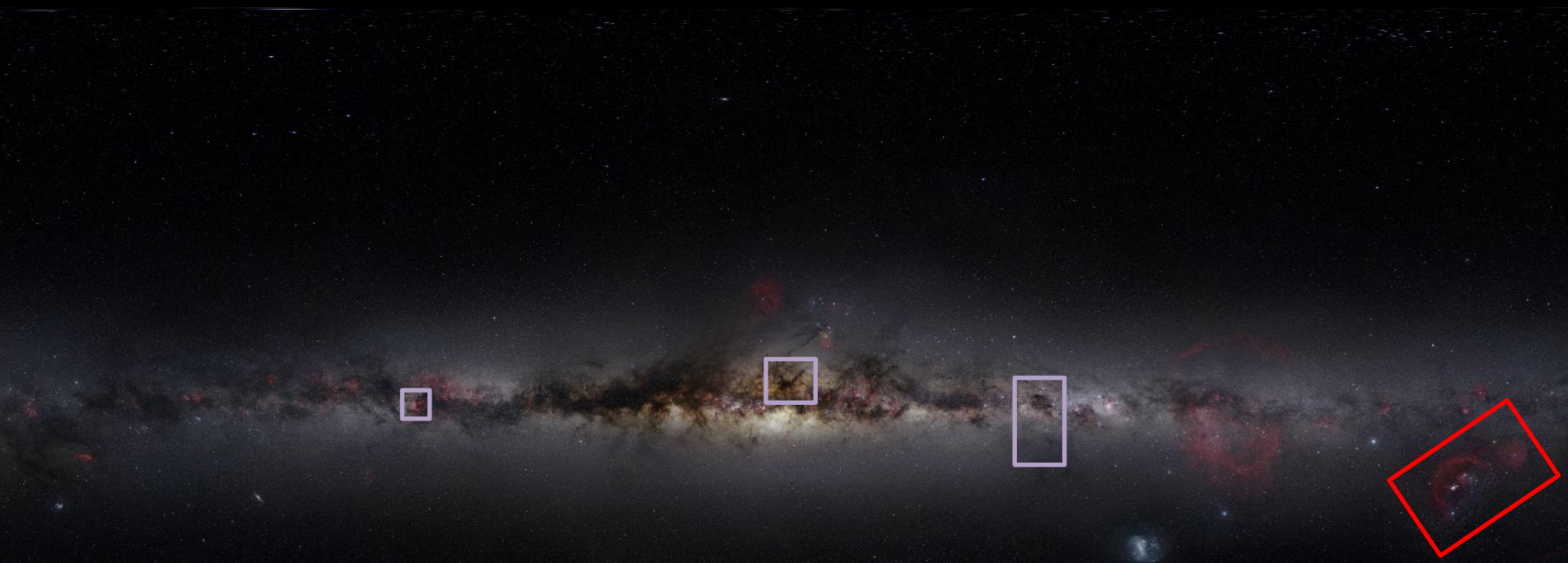
North America Nebula
(Norteamérica)



Coal Sack Nebula
(Saco de Carbón)



La Vía-Láctea en óptico/visible (cameras, 3000-7000 Å)

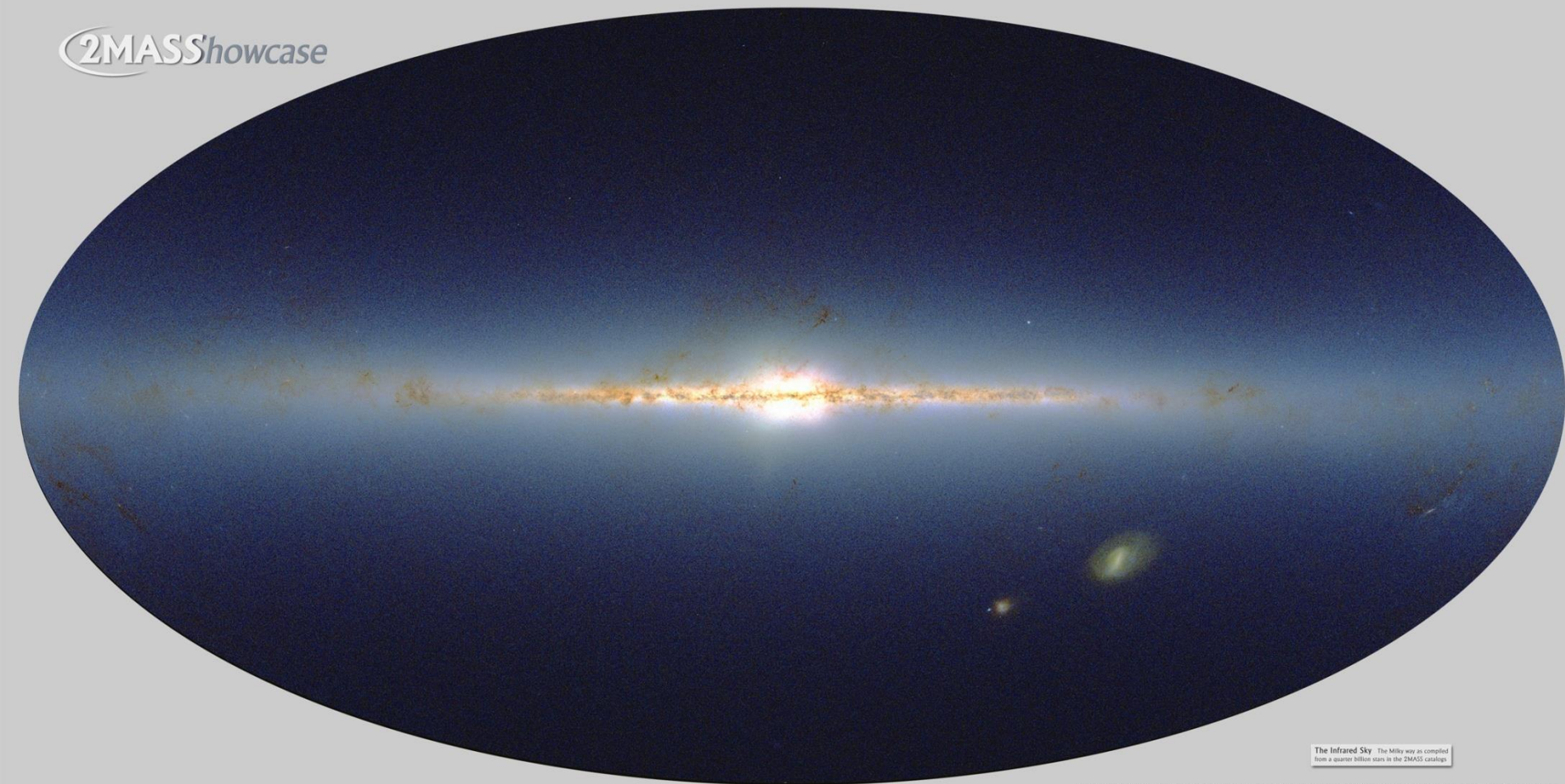


estrellas de temperatura intermedia (Seq. Principal), nubes moleculares (oscuras por el polvo)
+ nubes brillantes (líneas de emisión)



El cielo en infrarrojo cercano (telescopios 1.3m, ~2 μm)

2MASS Showcase

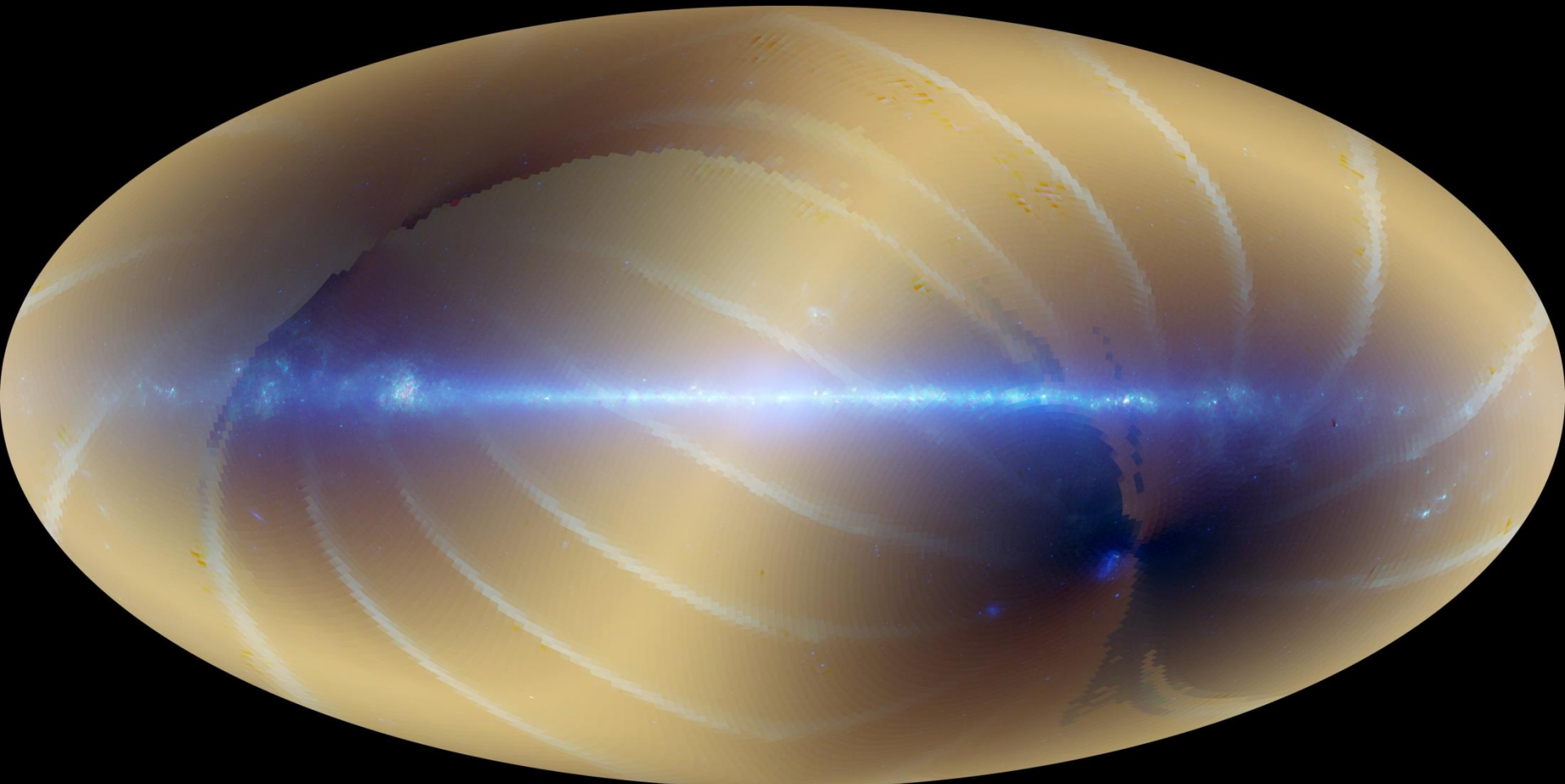


The Infrared Sky The Milky way as compiled from a quarter billion stars in the 2MASS catalog

Two Micron All Sky Survey Image Mosaic: Infrared Processing and Analysis Center/Caltech & University of Massachusetts

estrellas “frías” (Seq. Princ., gigantes)

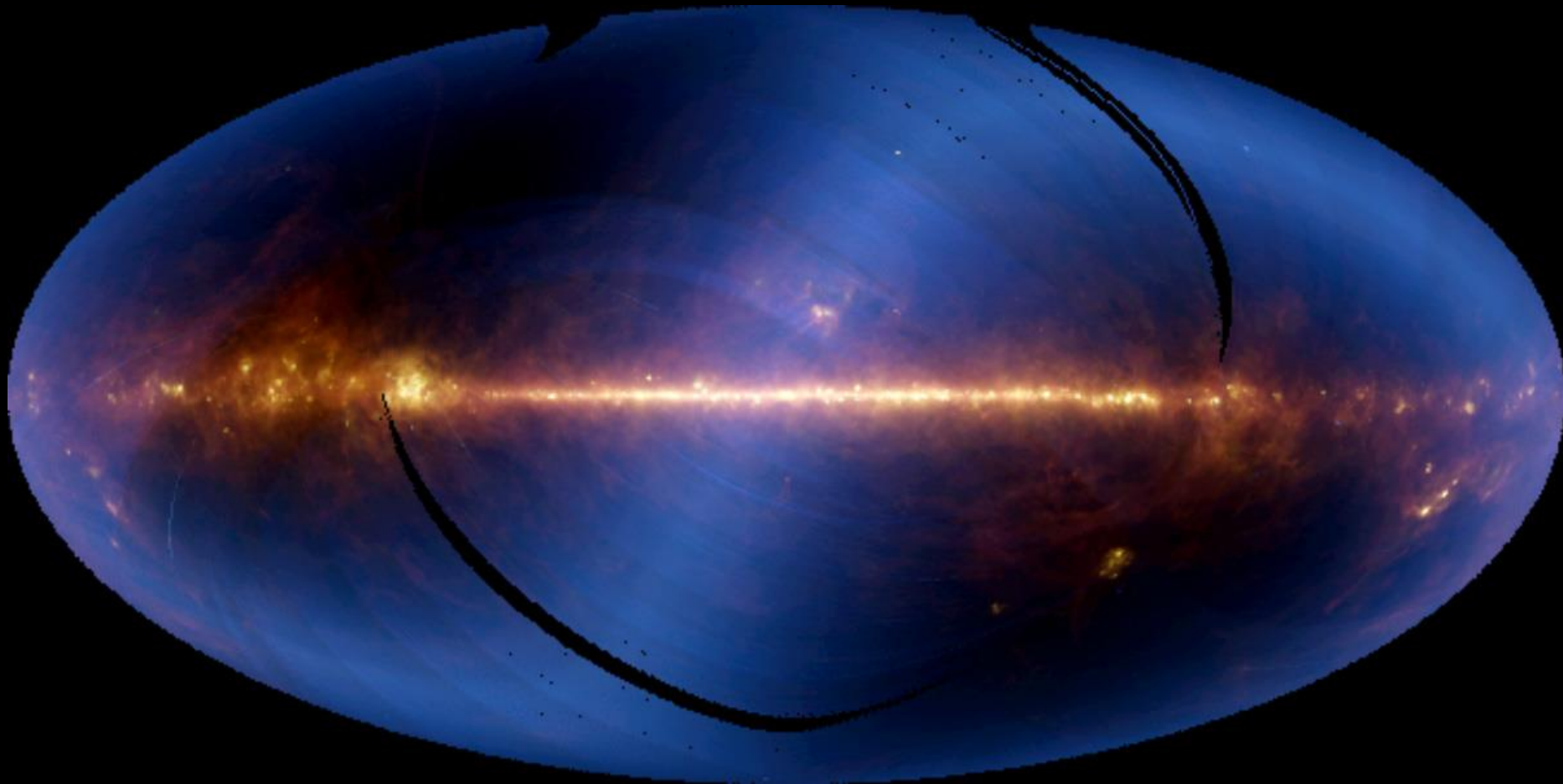
El cielo en el infrarrojo lejano (sat. WISE, 3-22 μm)



emisión de polvo caliente (regiones de formación estelar, Eclíptica)

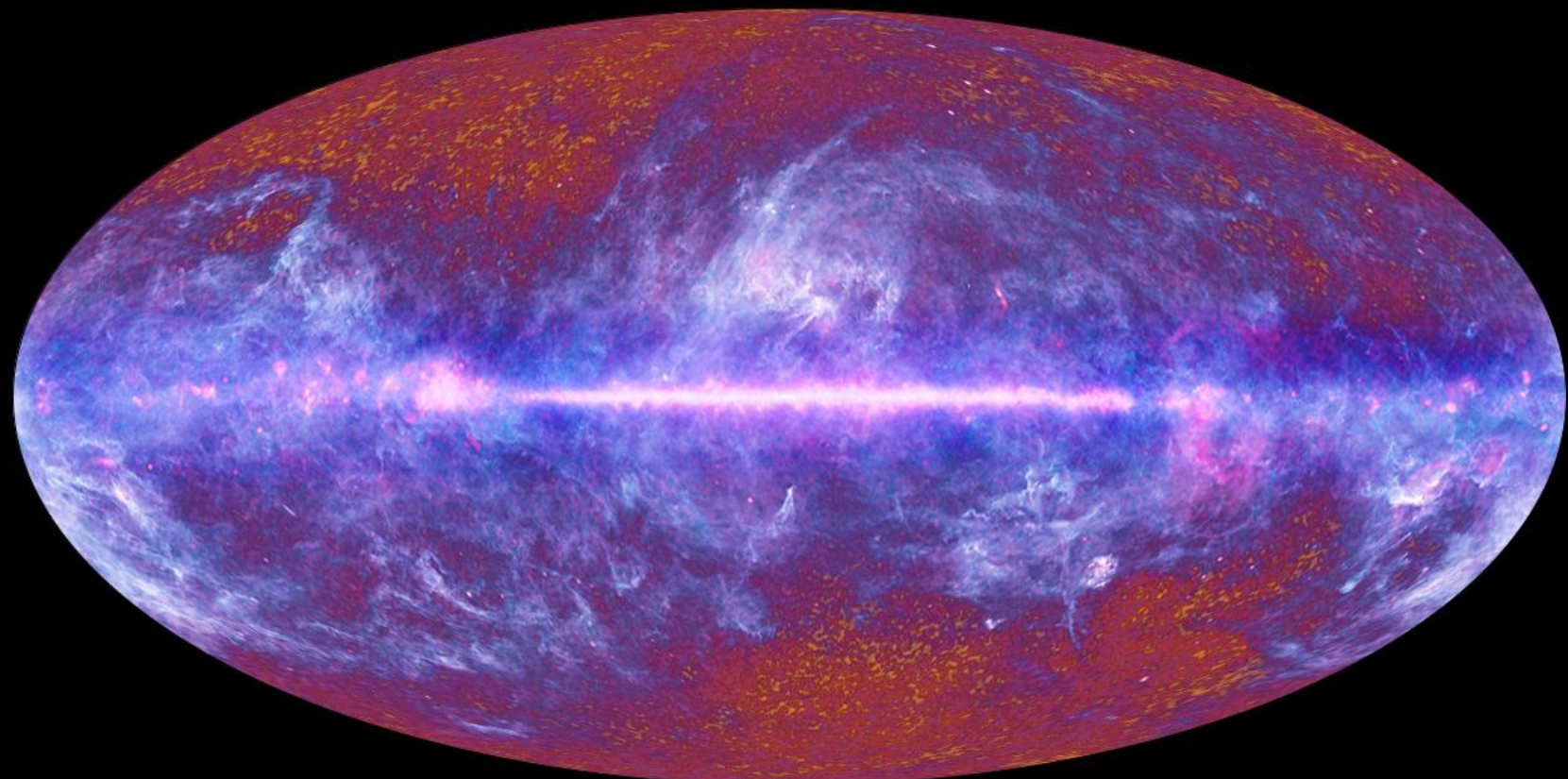


El cielo en el infrarrojo lejano (sat. IRAS, ~100 μm)



emisión de polvo caliente (regiones de formación estelar, Eclíptica)

El cielo en microondas (sat. Planck, 857-30 GHz = 0.35-10mm)

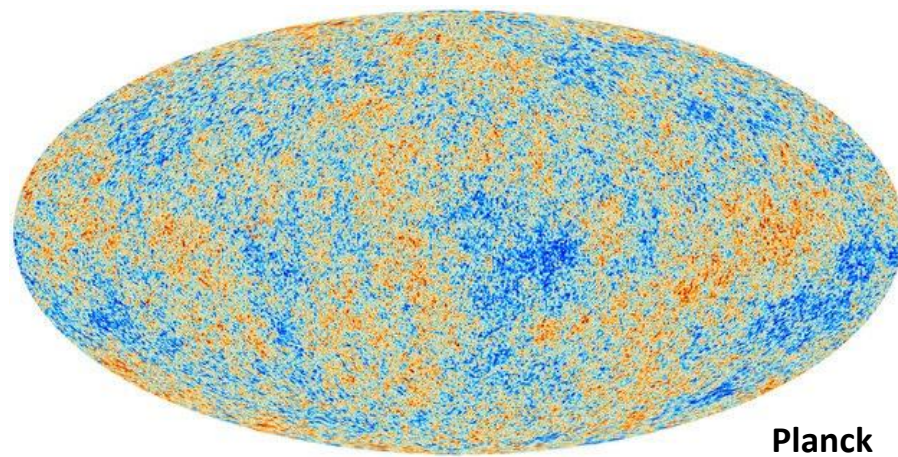
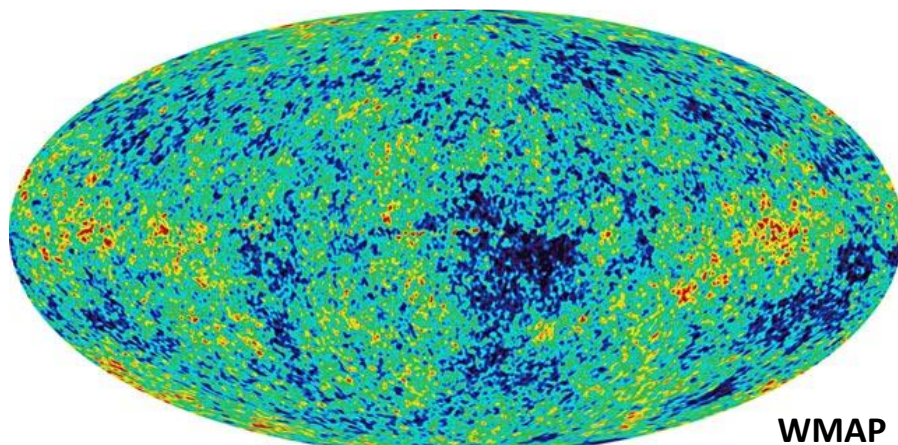
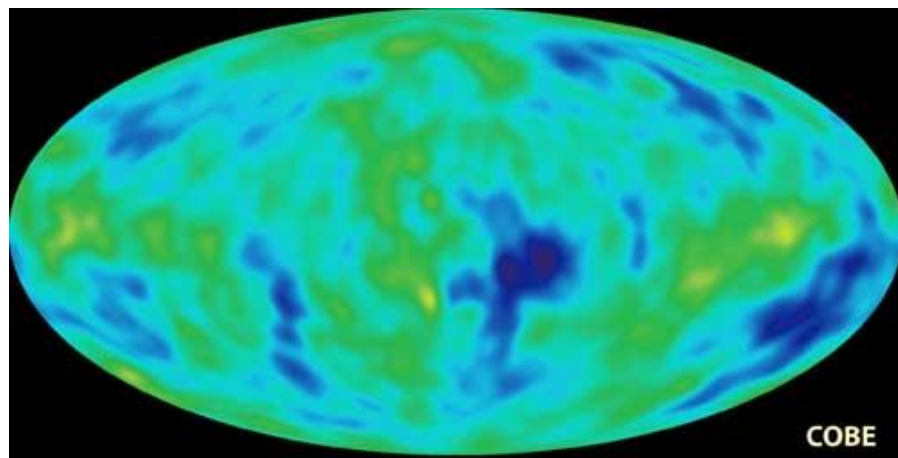
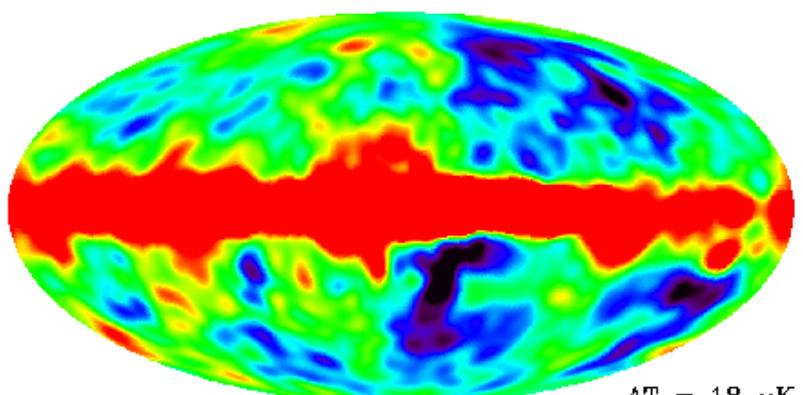
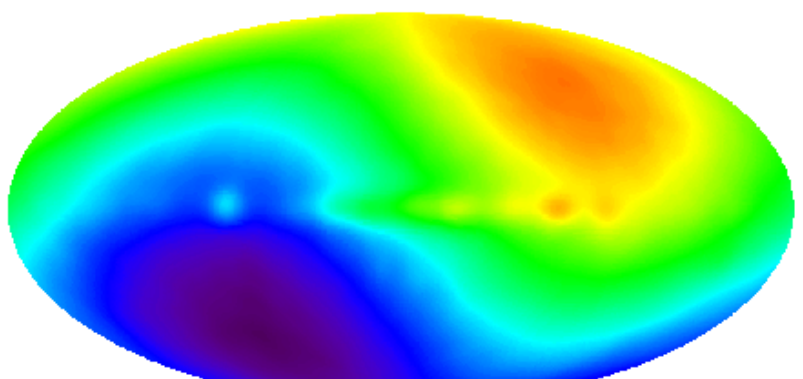
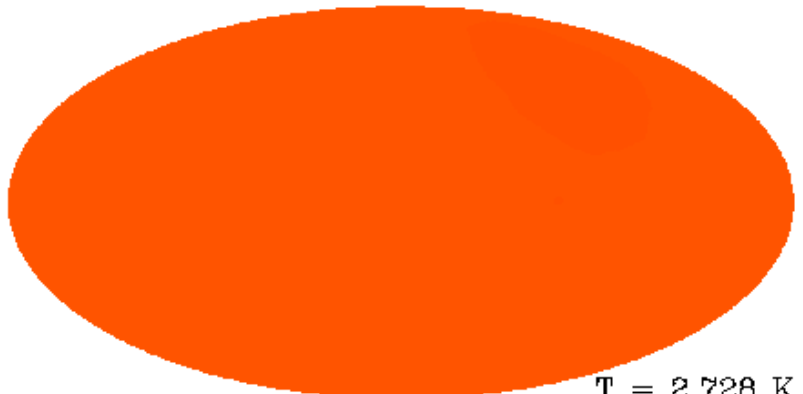


The Planck one-year all-sky survey

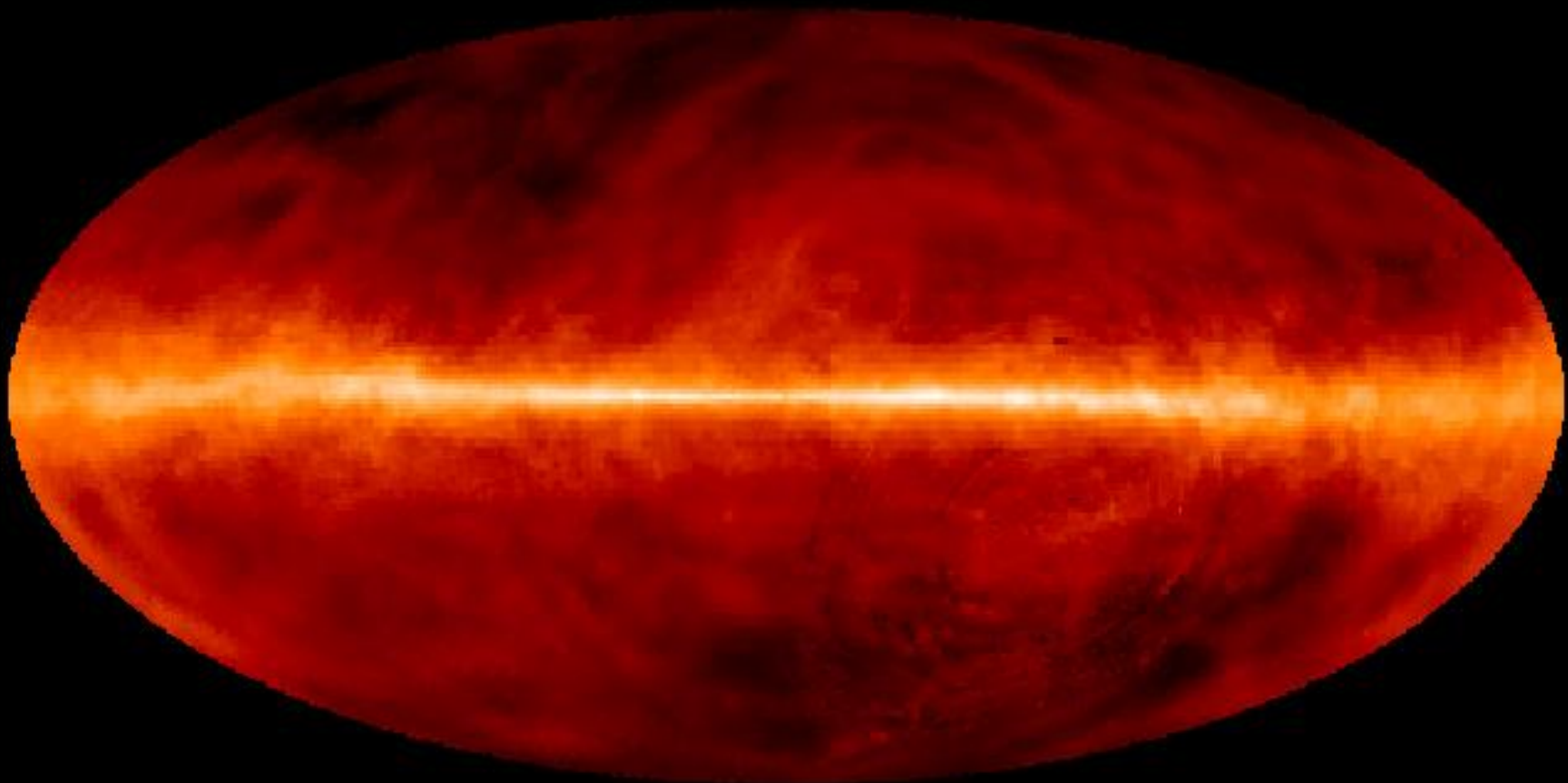


(c) ESA, HFI and LFI consortia, July 2010

transición entre emisión del polvo y sincrotrón del gas + CMB

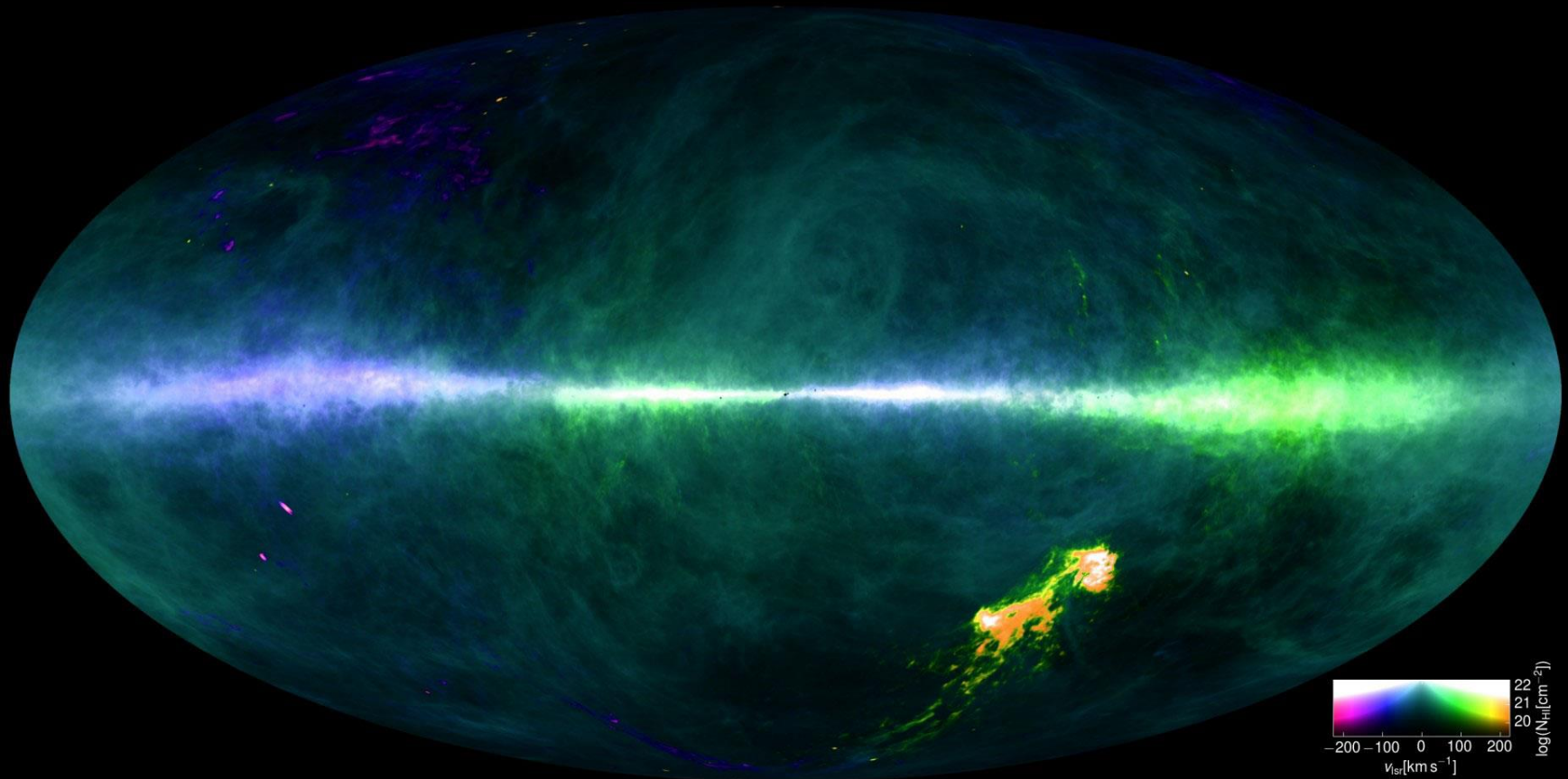


El cielo en radio (6 antenas, 1420 MHz = 21cm)



hidrógeno neutro (transición de spin)

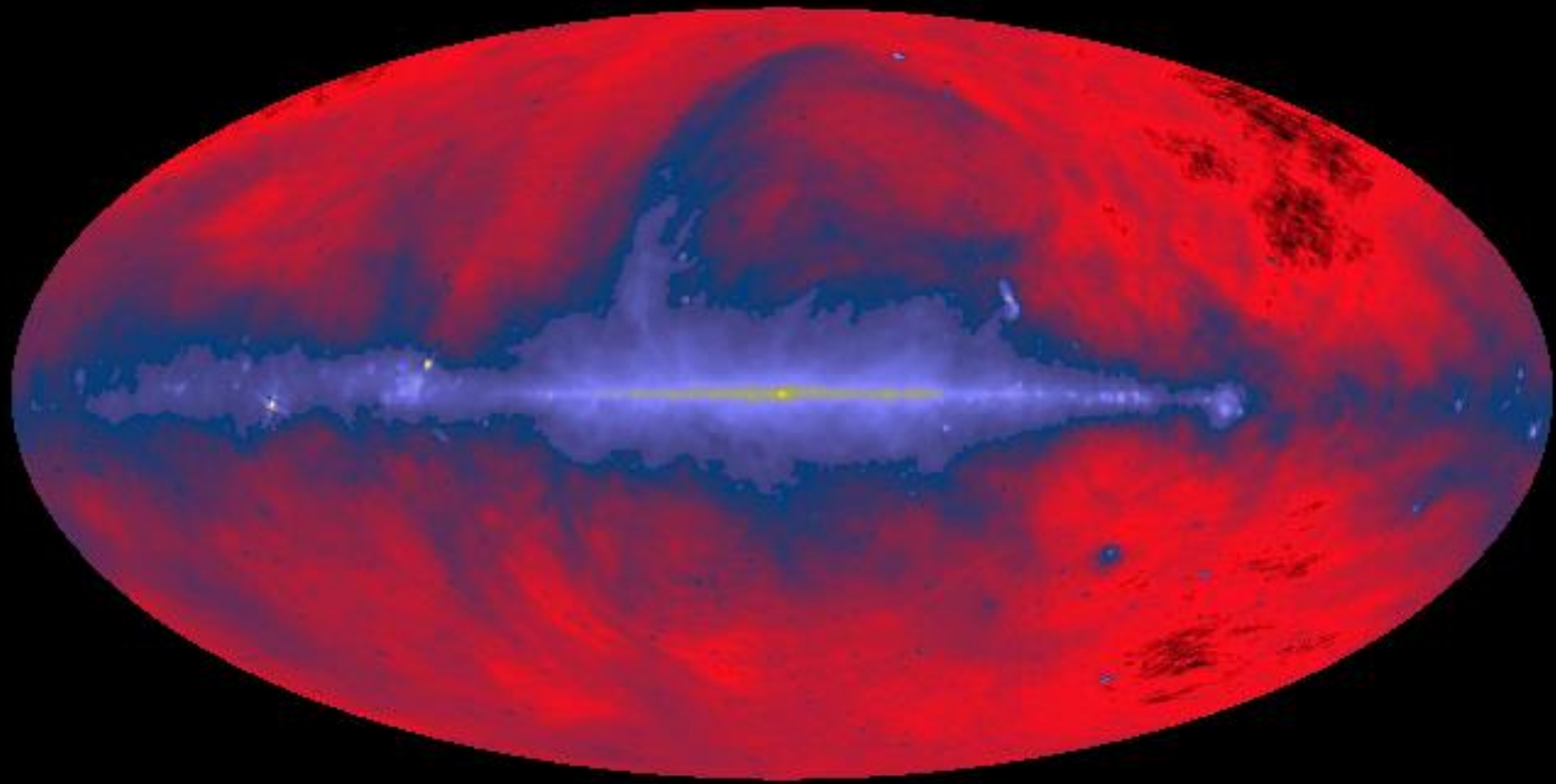
El cielo en radio (Effelsberg 100m + Parkes 64m, 1420 MHz = 21cm)



Benjamin Winkel & HI4PI Collaboration

hidrógeno neutro (transición de spin)

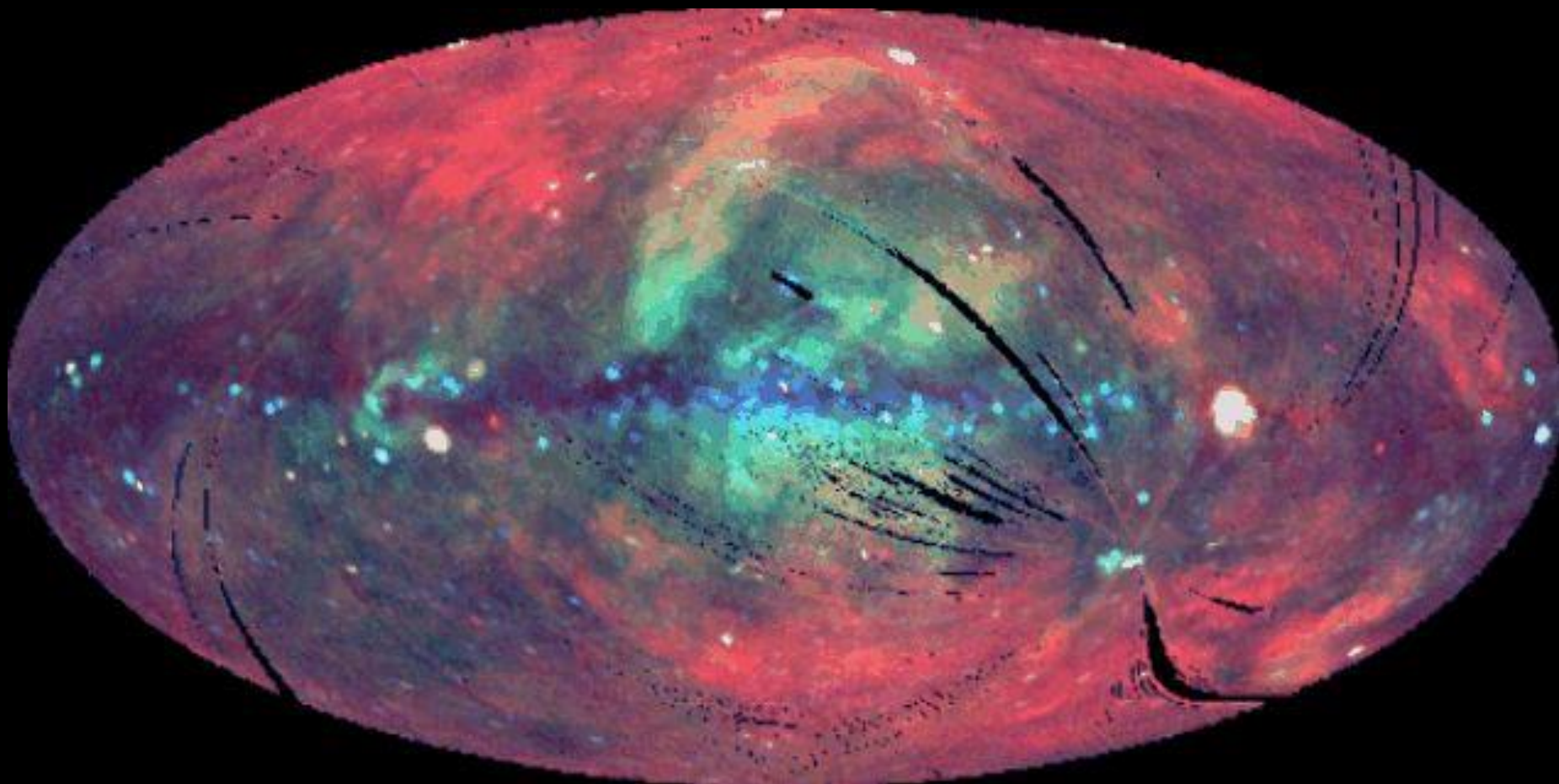
El cielo en radio (3 antenas, 64-100* m, 408MHz)



electrones en campos magnéticos - sincrotrón (pulsares, SNe, regiones de formación estelar)

* Parkes (Australia, 64m), Jodrell Bank (UK, 76m) y Effelsberg (Alemania, 100m)

El cielo en rayos-X (sat. ROSAT, 0.1-2.4 keV)

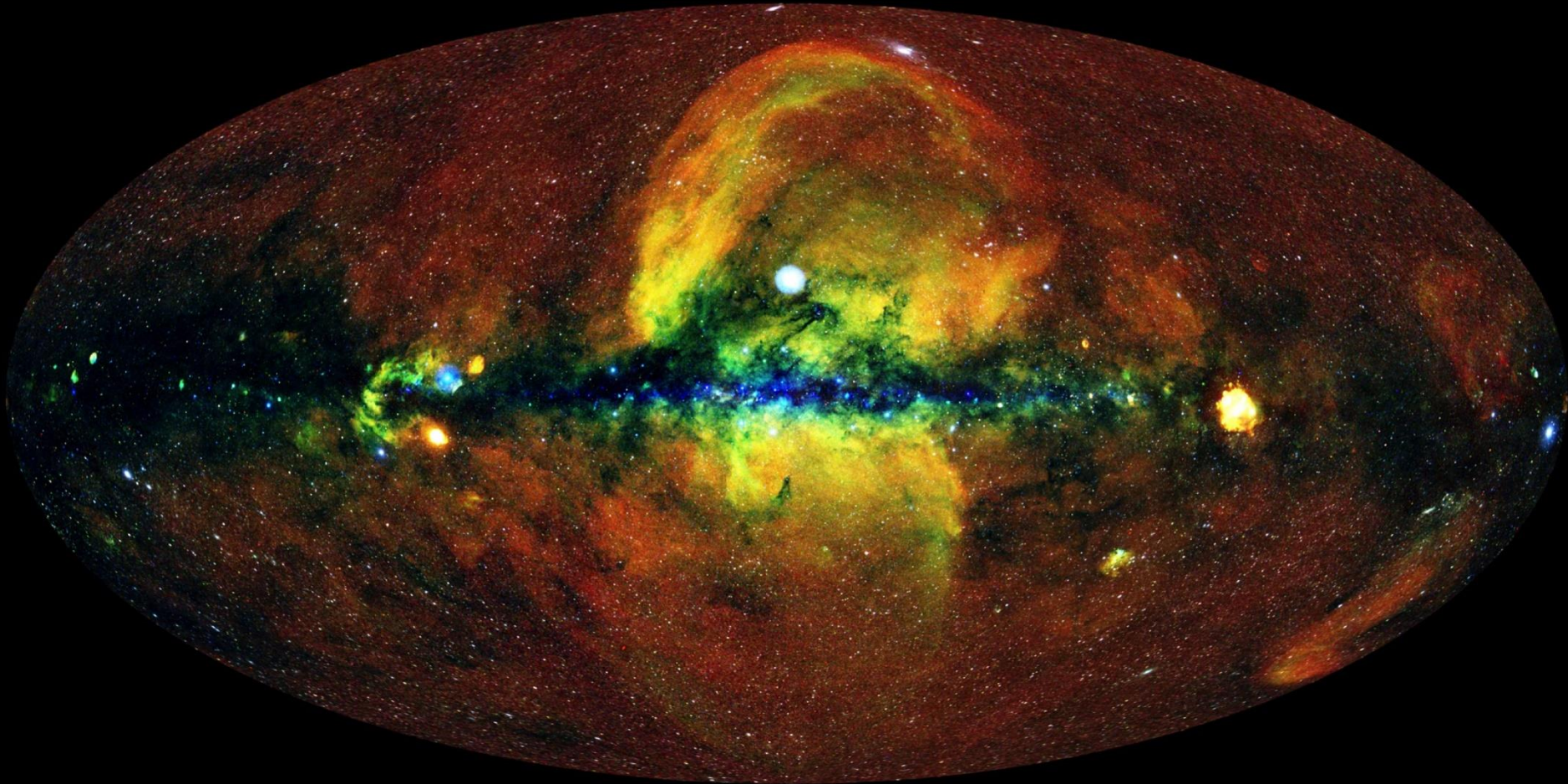


gas caliente, pulsares, galaxias activas (*bremsstrahlung* térmico)

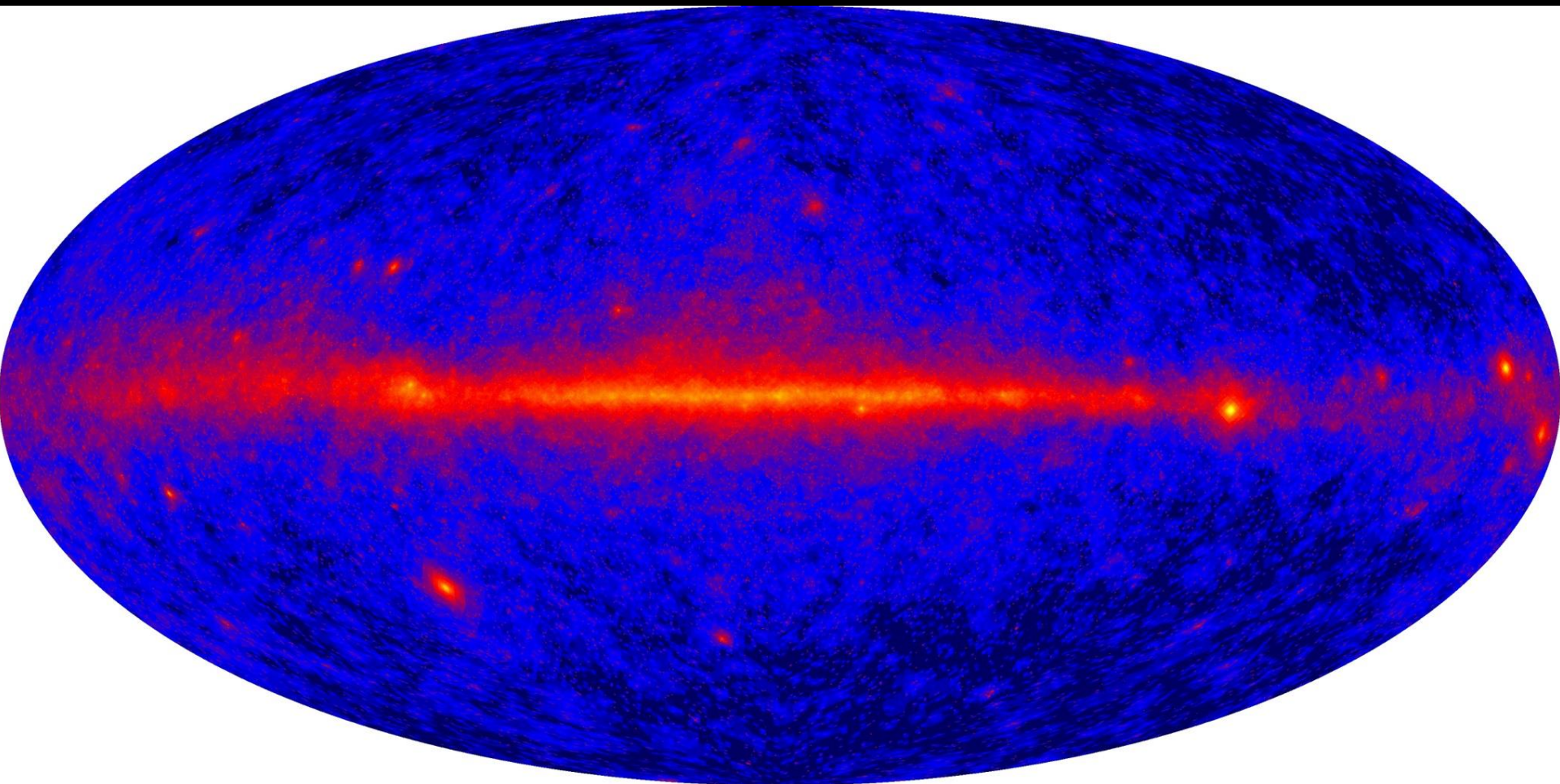
The X-ray sky from eROSITA



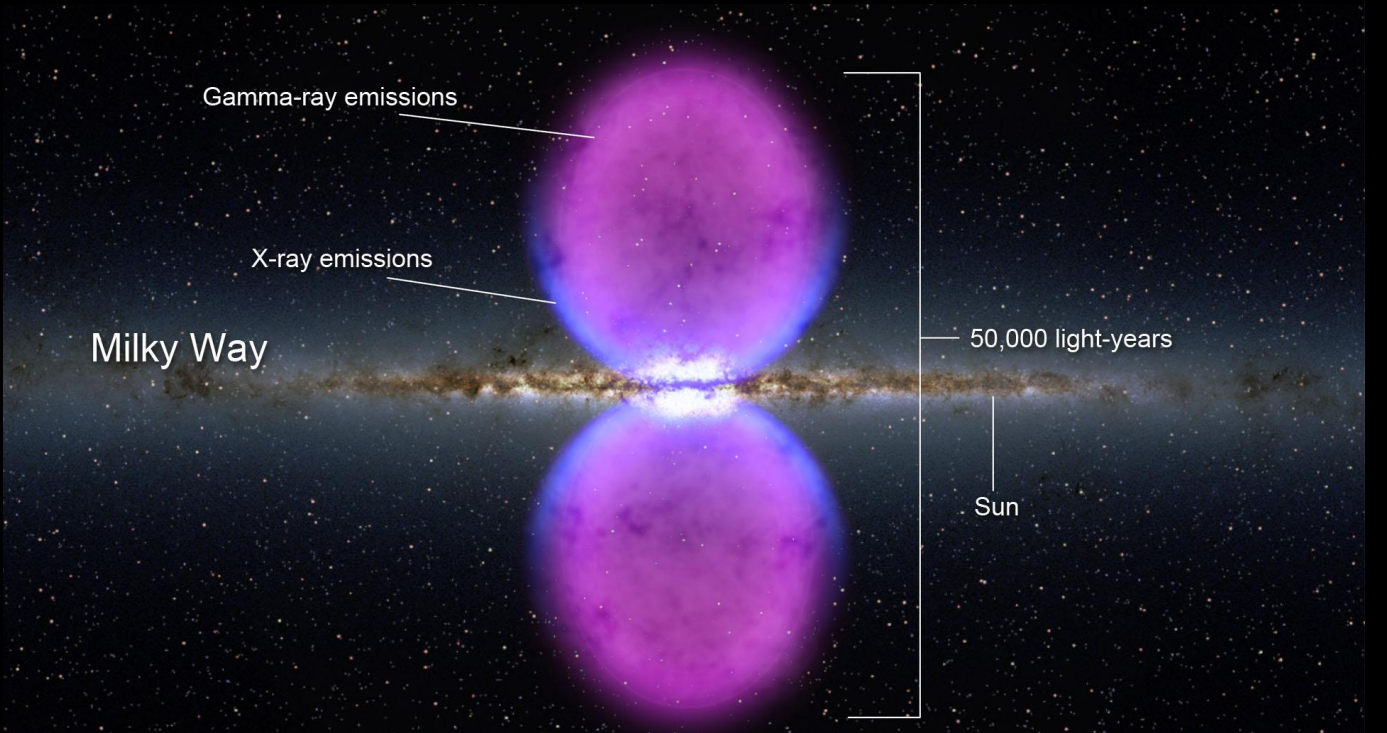
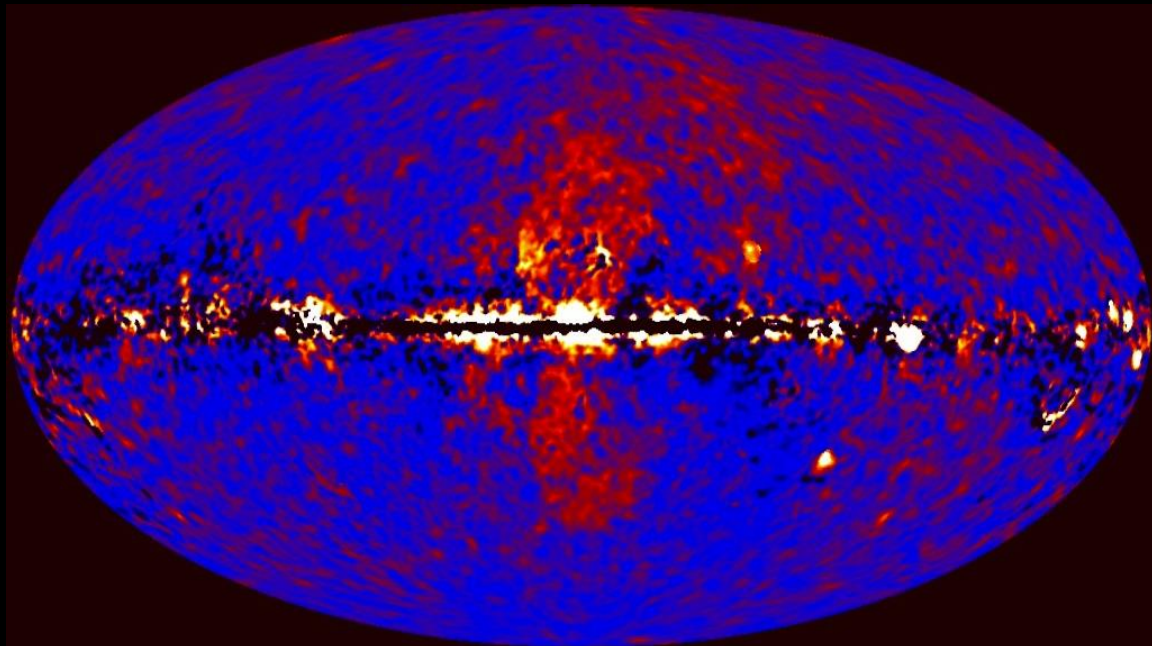
El cielo en rayos-X (eROSITA, L2 Point, 0.5-2 y 2-10 keV)



El cielo en rayos- γ (sat. Fermi GLAST, 30 keV-300 GeV)



Locales: explosiones solares; Galácticas: pulsares, remanentes de SNe, binarias rayos-X, micro-cuásares; Extragalácticas: galaxias SB, AGNs, brotes de rayos- γ



Conceptos Básicos 3

- Color

★ índices de color

$$m_A - m_B = \text{cte.} - 2.5 \log [\int d\lambda S_\lambda(A) f_\lambda] / [\int d\lambda S_\lambda(B) f_\lambda]$$

- Metalicidad

X → H

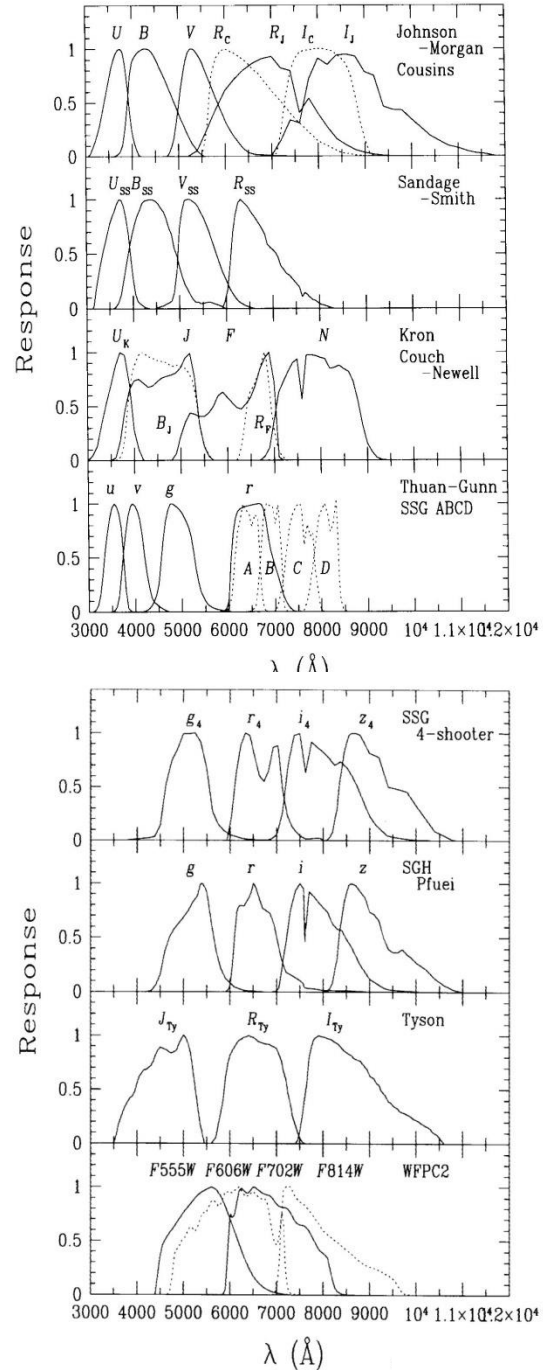
Y → He

Z → “metales”

★ Estimadores usuales

$$[\text{Fe}/\text{H}] = \log \frac{(\text{Fe}/\text{H})_*}{(\text{Fe}/\text{H})_\odot} = \log (\text{Fe}/\text{H})_* - \log (\text{Fe}/\text{H})_\odot$$

$$\{12 + \log(\text{O}/\text{H})\}_\odot = 8.91$$



Sistema de coordenadas cilíndricas:

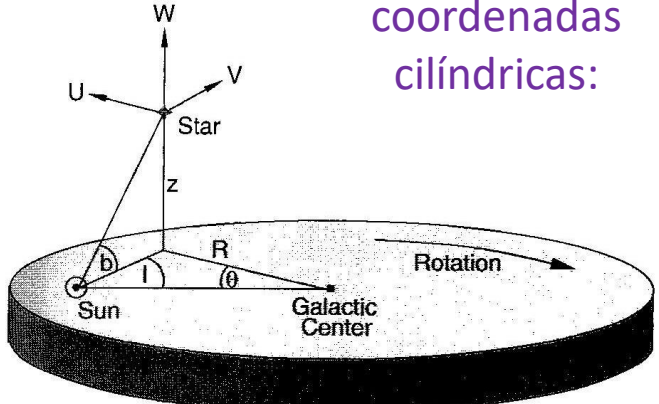


Fig. 2.13. Cylindrical coordinate system (R, θ, z) with the Galactic center at its origin. Note that θ increases in the clockwise direction if the disk is viewed from above. The corresponding velocity components (U, V, W) of a star are indicated

Densidad numérica en la dirección perpendicular al disco Galáctico:

$$n(z) \propto \exp(-|z|/h_z)$$

$h_z \rightarrow$ escala de altura (distancia en la cual la densidad baja $1/e$ de su valor central)

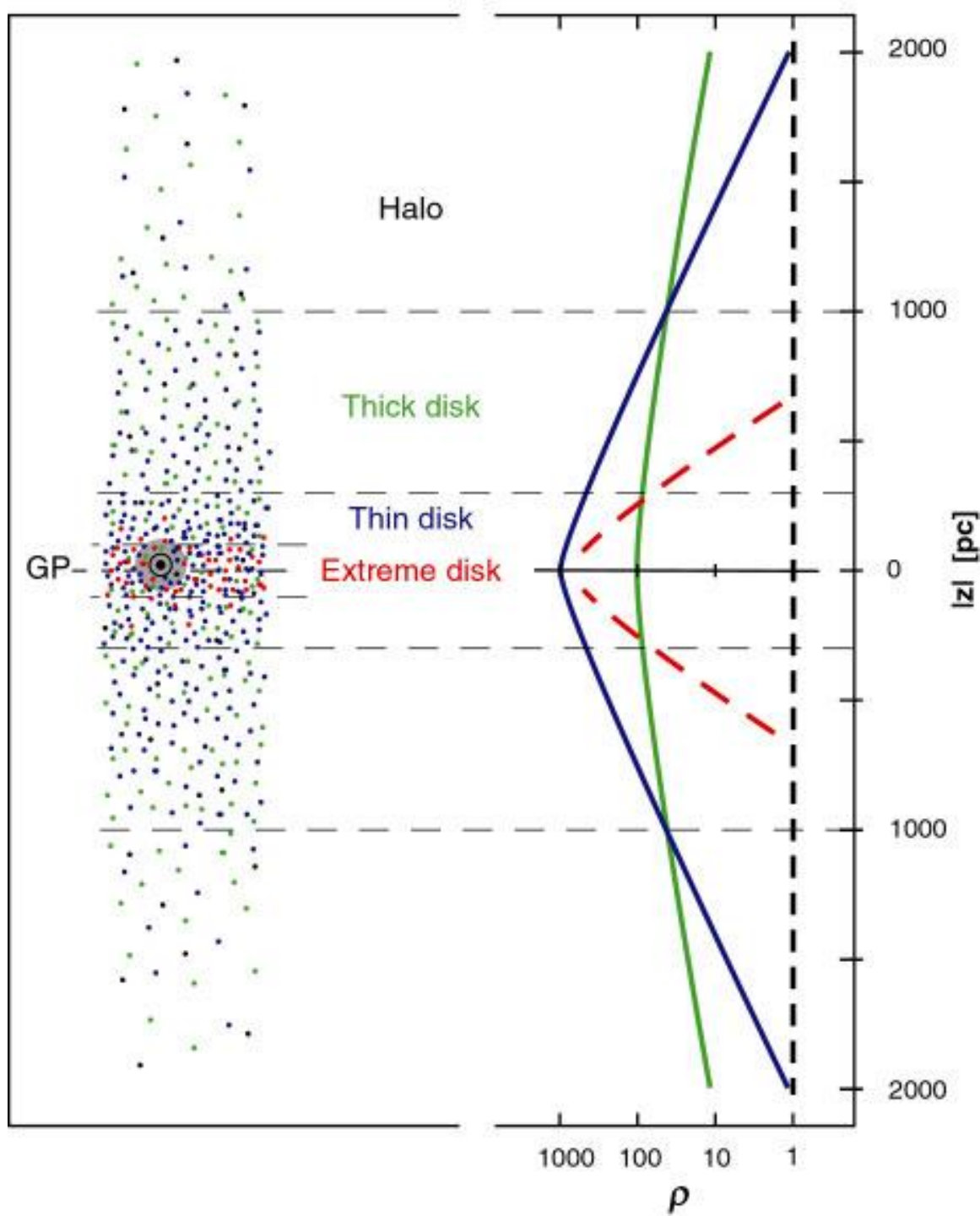


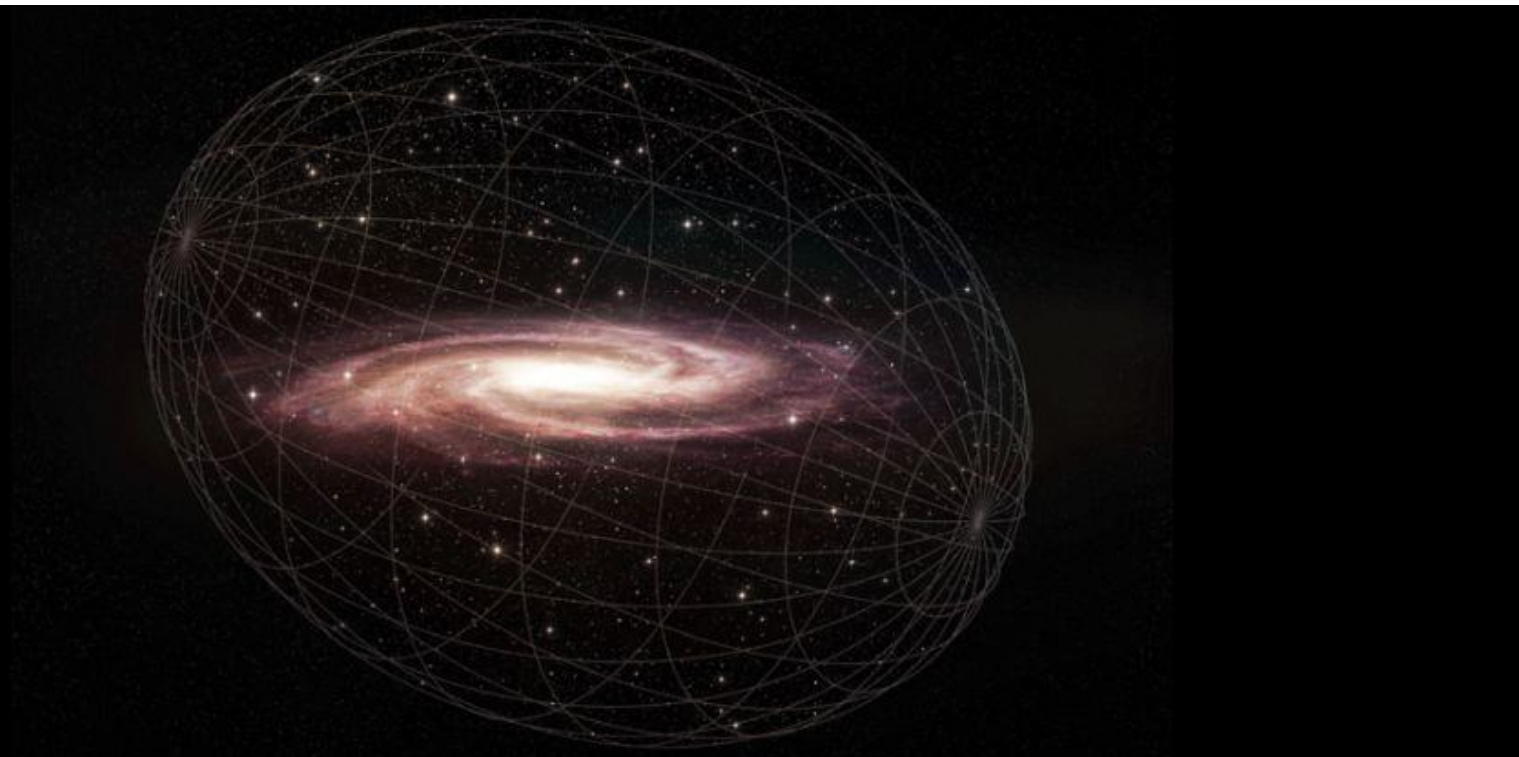
Table 2.1 Scale heights and velocities of gas and stars in the disk and halo

<i>Galactic component</i>	h_z (pc)	σ_R (km s $^{-1}$)	σ_ϕ (km s $^{-1}$)	σ_z (km s $^{-1}$)	$\langle v_y \rangle$ (km s $^{-1}$)
HI gas near the Sun	130		≈ 5	≈ 7	tiny
Local CO, H ₂ gas	65		4		tiny
Disk stars: $Z > Z_\odot/4$		(Fig. 2.8)			
$\tau < 3$ Gyr	≈ 250	30	21	16	-11
$3 < \tau < 6$ Gyr	≈ 300	36	25	19	-9
$6 < \tau < 10$ Gyr	≈ 350	38	25	24	-16
$\tau > 10$ Gyr		62	52	37	-21
Thick disk					
[Fe/H] > -0.8	~ 1500	52	37	40	-35
Halo stars near Sun					
[Fe/H] < -1.6	$\gtrsim 1$ kpc	~ 150	~ 100	~ 100	-210
Halo stars at $2.5R_0$	few kpc	80–100	130–150	130–150	-220

Note: Gas velocities are measured looking up out of the disk (σ_z of HI), or at the tangent point (σ_ϕ for HI and CO); velocities of thin disk stars refer to F stars of Figure 2.8.

Velocity v_y is in the direction of Galactic rotation, relative to the *local standard of rest*, a circular orbit at the Sun's radius R_0 , assuming $v_{y,\odot} = 5$ km s $^{-1}$.

El Halo

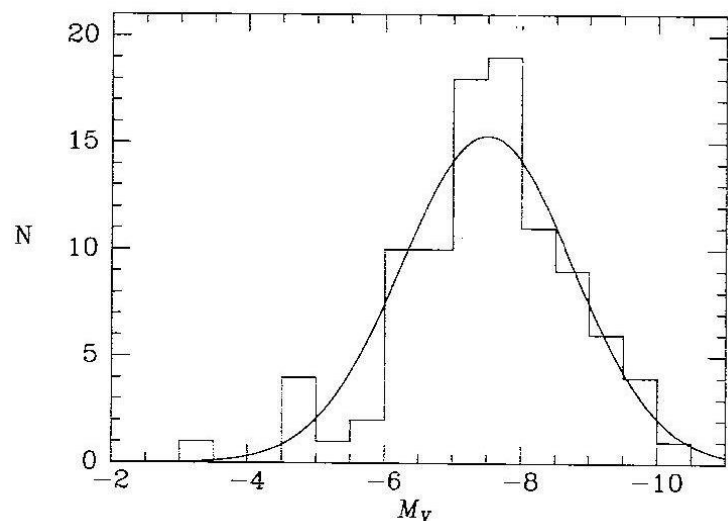
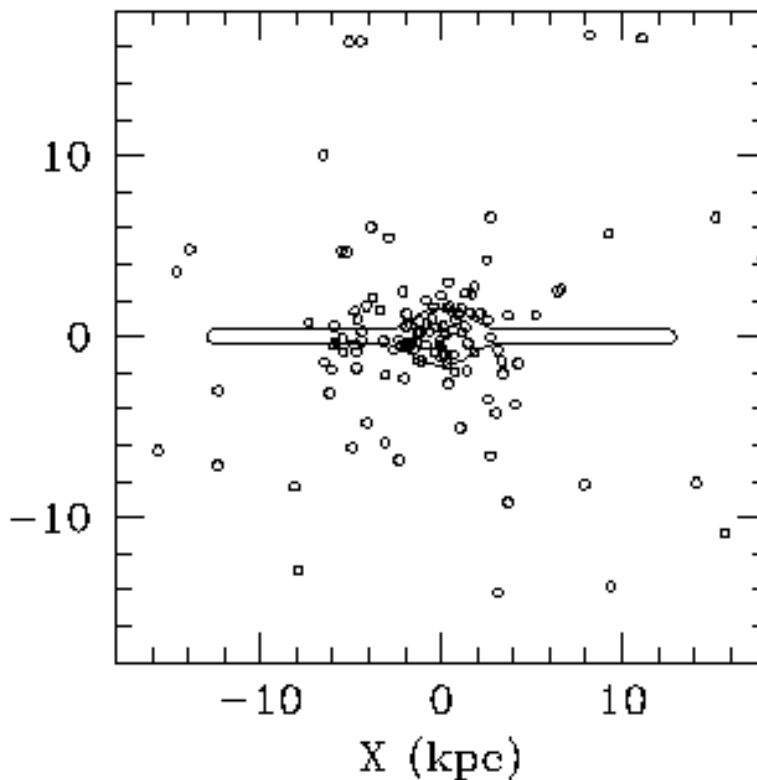
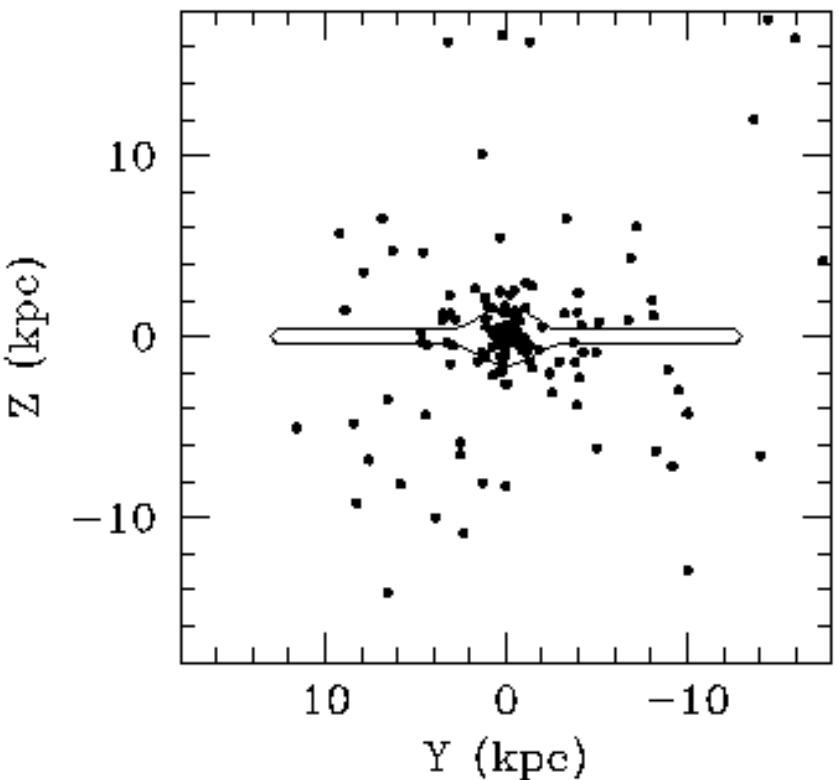


Sistema de Cúmulos Globulares

- ~ **160** conocidos
- $r_{CG} \sim 20$ pc
- distribución ~ esférica ($R > 40$ kpc)
- FL Gaussiana (vela estándar)

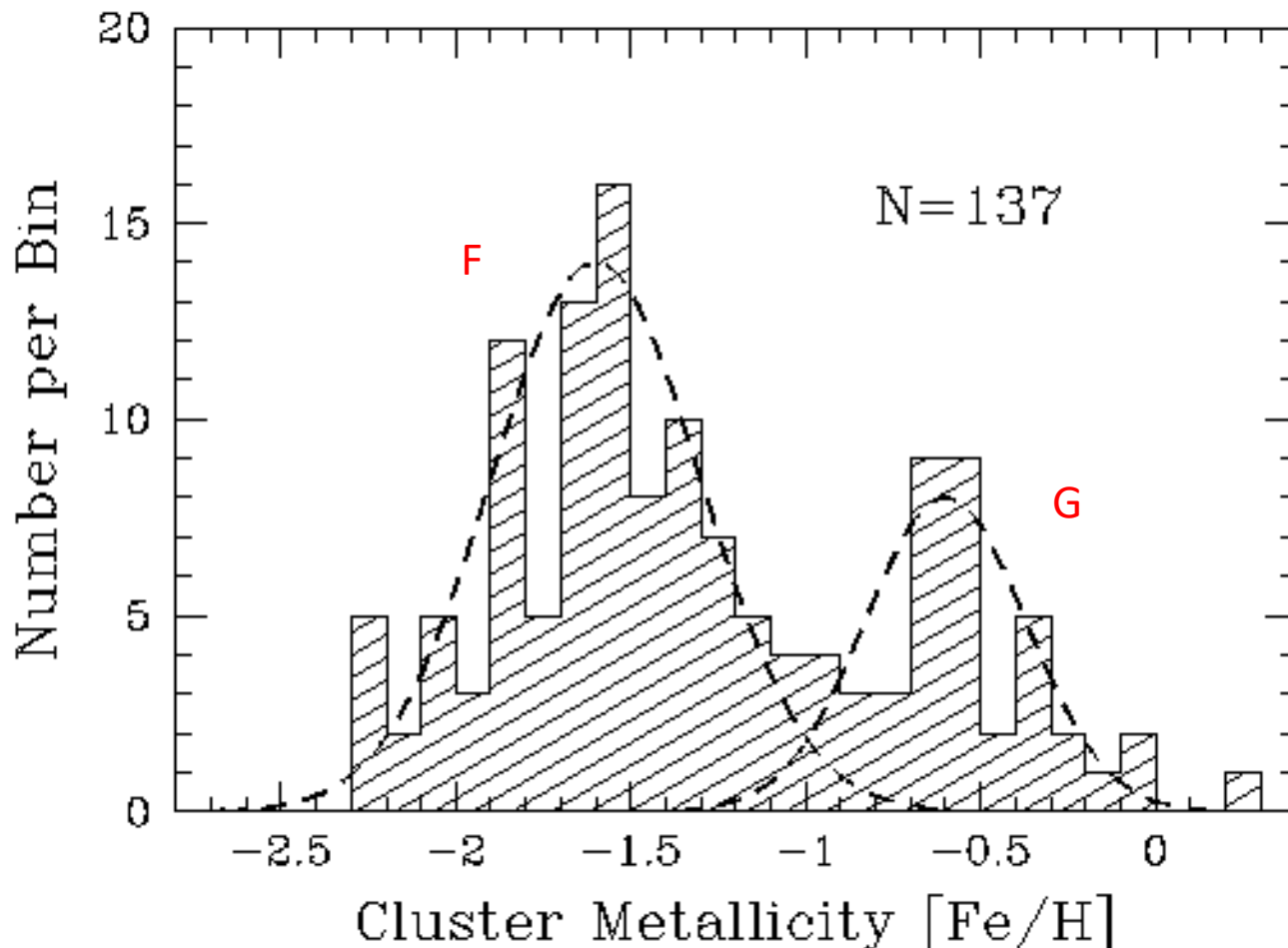
Harris *et al.* 1996, AJ 112, 1487
(last update: 2010)

<https://physics.mcmaster.ca/~harris/mwgc.dat>



Cúmulos Globulares

- dos poblaciones :
 - $[\text{Fe}/\text{H}] < -0.8 \rightarrow$ pobres en metales, viejos, \in halo (Cúmulos **F**)
 - $[\text{Fe}/\text{H}] > -0.8 \rightarrow$ ricos en metales, jóvenes, \in disco (Cúmulos **G**)
distribución mas achatada, mayor rotación



Kinman (1959)
MNRAS 119, 559
Zinn (1985)
ApJ 293, 424
Armandroff (1989)
AJ 97, 375

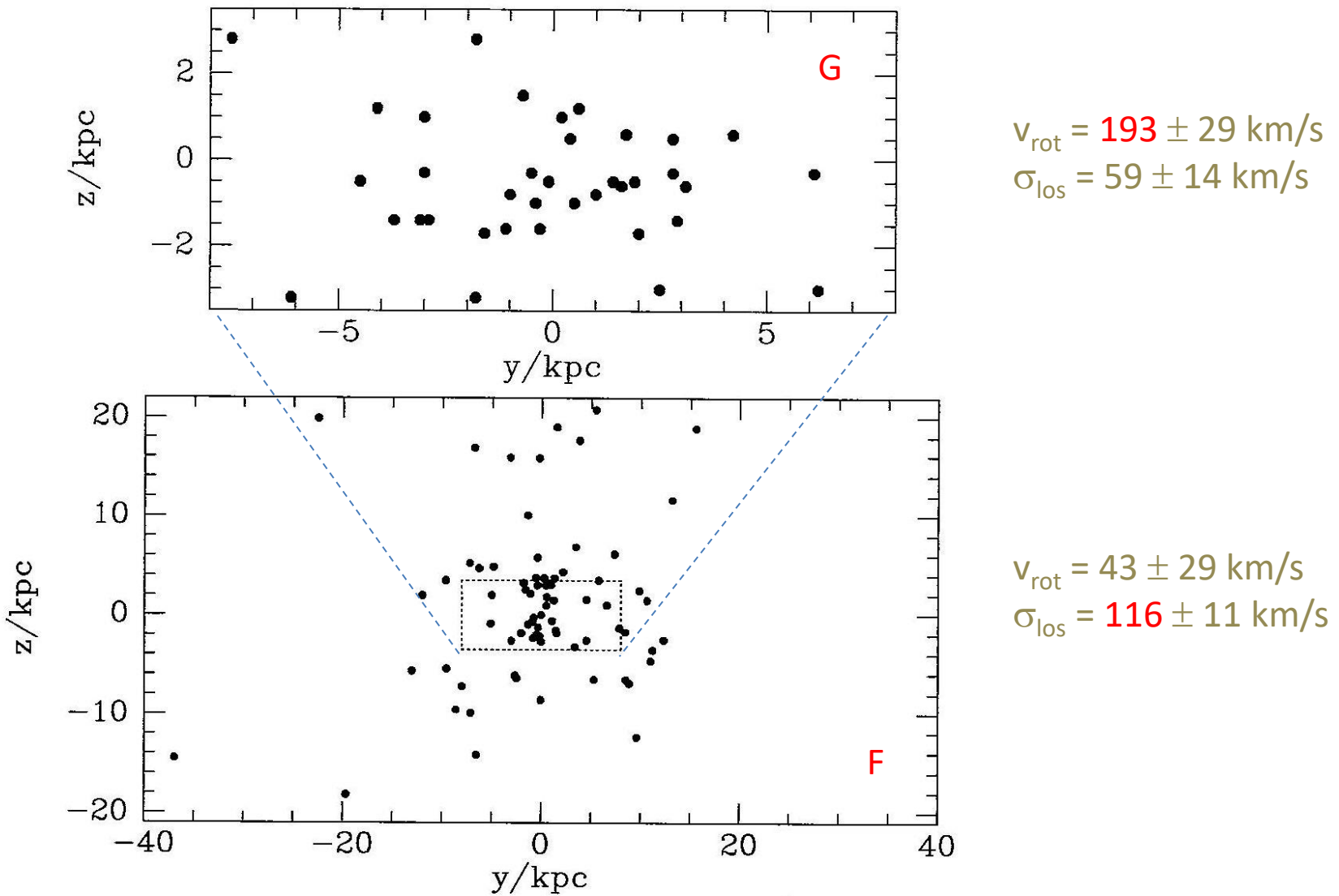


Figure 10.30 The distribution of the disk (top) and halo (bottom) globular clusters as viewed by an observer located at a large distance in the anticenter direction. The dotted rectangle in the lower panel indicates the region shown in the upper panel. In the upper panel we have superimposed the distribution that would be seen by an observer located at a large distance in the direction $l = 270^\circ$. In each panel the Galactic center lies at the origin. [From data published in Armandroff (1989)]

Estrellas de Campo del Halo

- $R \sim 25 \text{ kpc}$ ($h = 3 \text{ kpc}$)
- muy pobres en metales (parecidas a las de Cúmulos Globulares)
- búsqueda:
 - RRLyrae con periodos similares a los de esas estrellas en CGlob.
 - estrellas del HB
 - estrellas con movimientos propios muy altos
- proveen informaciones a cerca del origen de la VL
- determinación de la distancia del Sol al centro galáctico (R_0)

- IAU, 1985: $R_0 = 8.5 \text{ kpc}$
- Mediciones mas recientes
 $R_0 \sim 8 \text{ kpc}$

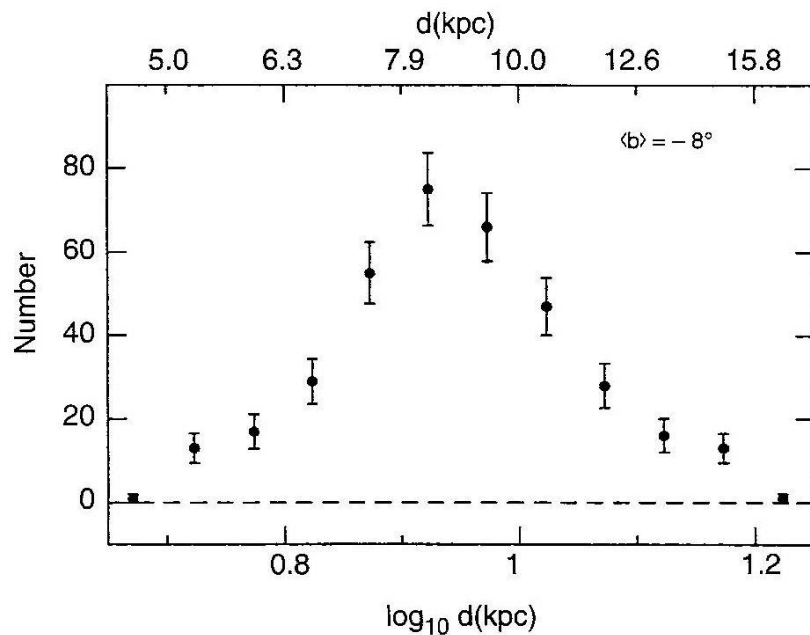


Fig. 2.12. The number of RR Lyrae stars as a function of distance, measured in a direction that closely passes the Galactic center, at $\ell = 0^\circ$ and $b = -8^\circ$. If we assume a spherically symmetric distribution of the RR Lyrae stars, concentrated towards the center, the distance to the Galactic center can be identified with the maximum of this distribution

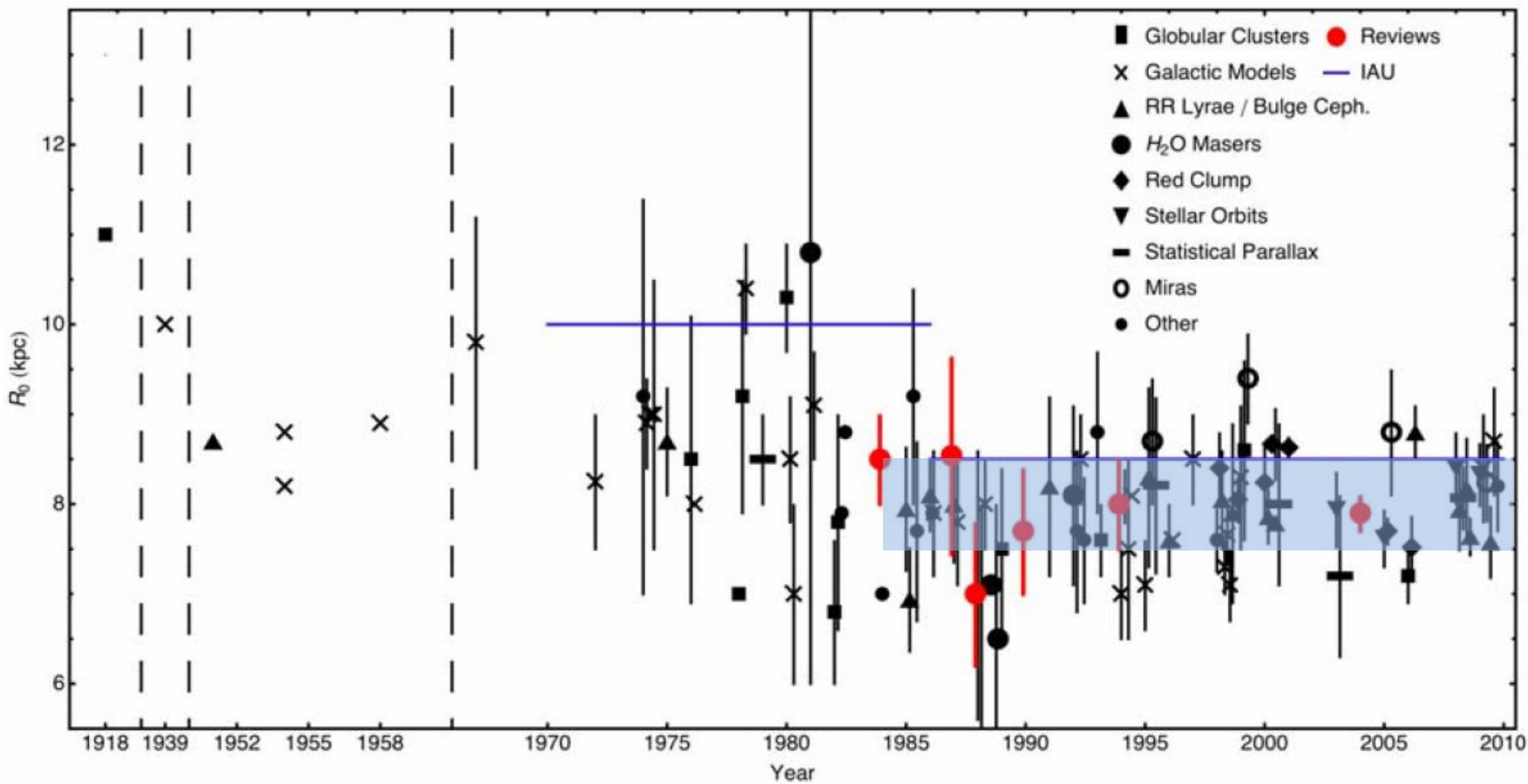
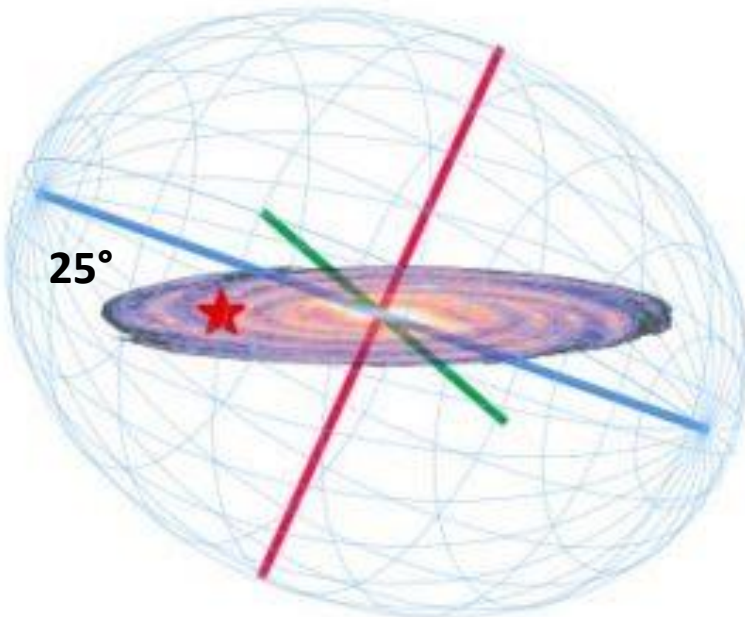
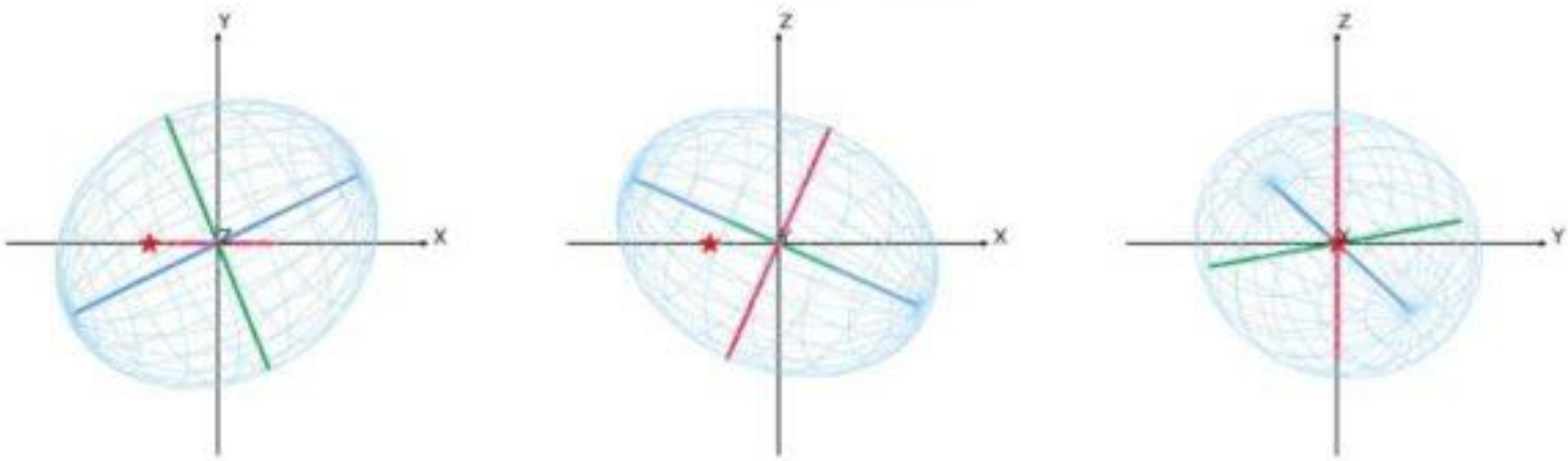


Figure 5.5.1: Graphical compilation of published values for R_0 . The publication dates have been adjusted slightly such that the overlap between the various error bars is minimized. The time axis before 1970 has three gaps from 1920 to 1938, 1940 to 1950 and 1960 to 1970, denoted by vertical, dashed lines.



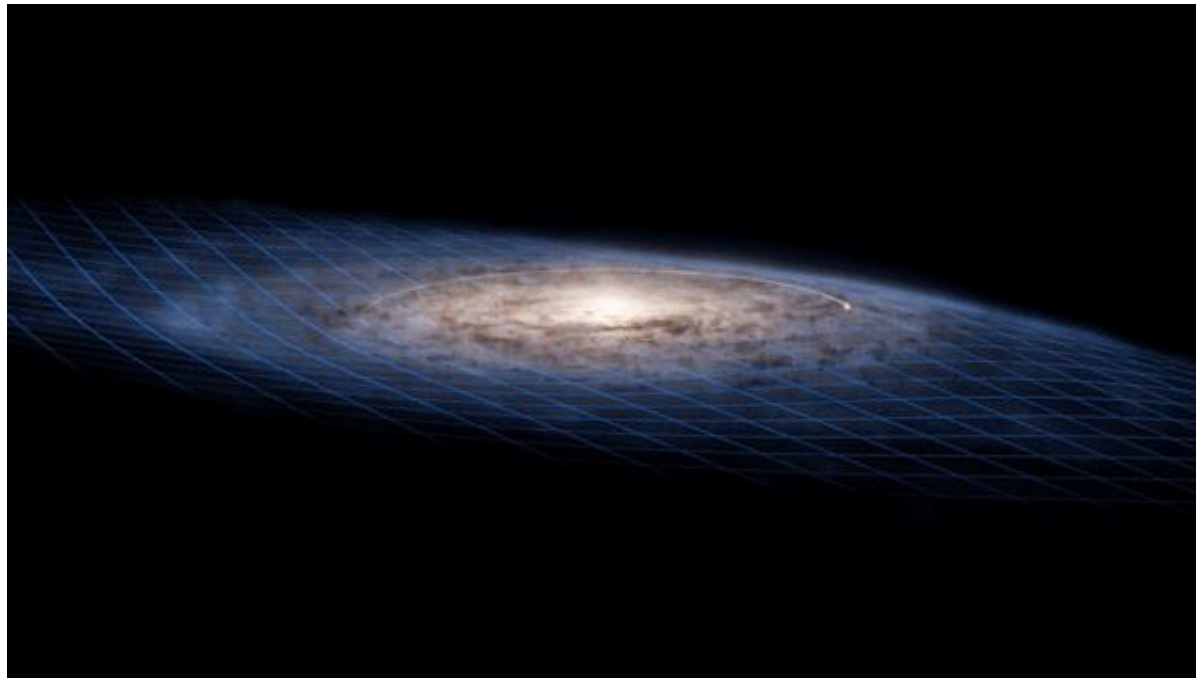
Axis Ratios
10 : 8 : 7



Gaia + H3

(Hectochelle in the Halo at High Resolution, MMT)

Han *et al.* 2022, AJ 164, 249



El Disco

Dispersiones de velocidades

- el movimiento aleatorio de las estrellas, σ , es dependiente del tipo de estrella (color, metalicidad, edad)
- las estrellas mas viejas (rojas y de menor [Fe/H]) tienen mayor σ
- se supone que todas nacen con bajos σ , pero gradualm/e van calentándose por procesos dinámicos en acción en el disco (dispersión por GMC, excitación por la estructura espiral, etc).

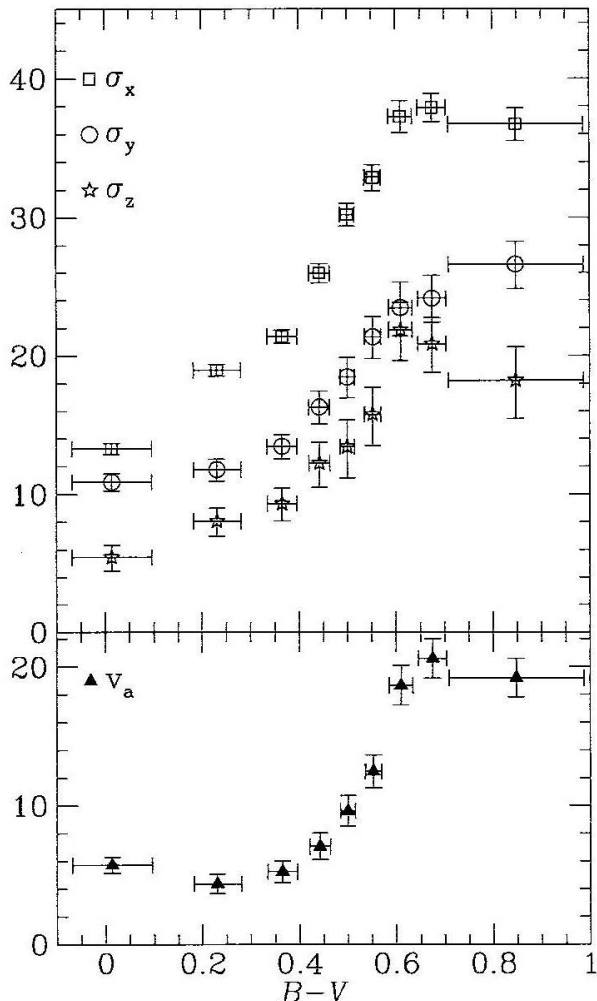


Figure 10.12 Top panel: the principal velocity dispersions σ_x , σ_y , σ_z of MS stars as a function of $B - V$. Bottom panel: the asymmetric drift, V_a , of MS stars as a function of $B - V$. [After Dehnen & Binney (1998a)]

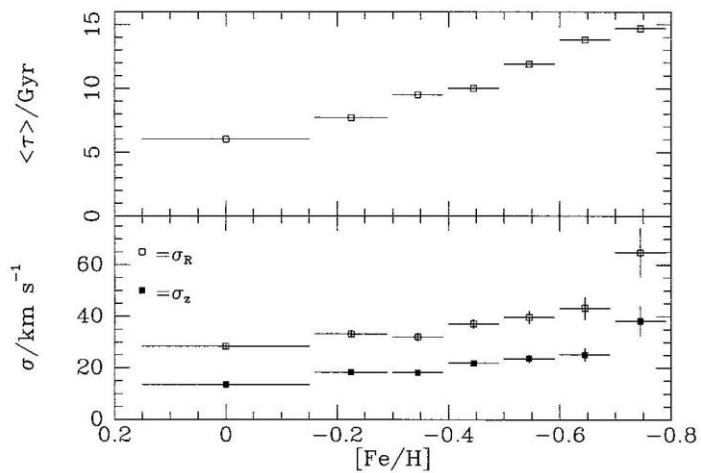


Figure 10.21 The dispersions in v_R and v_z and the mean age $\langle \tau \rangle$ of 1294 stars binned by metallicity. [From data published in Strömgren (1987)]

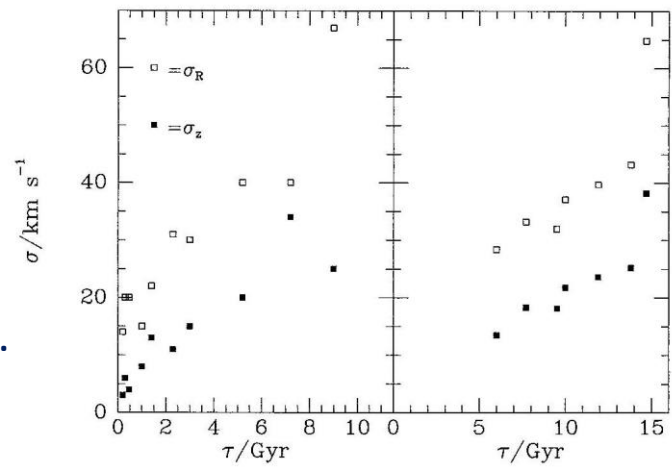
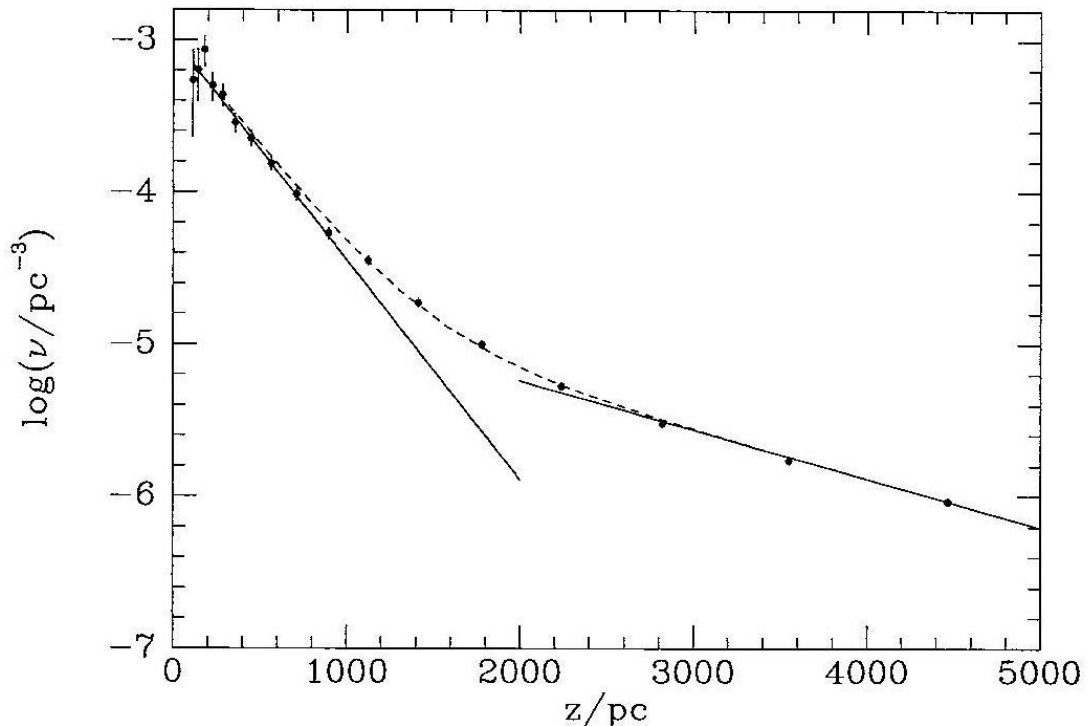


Figure 10.20 Velocity dispersion versus age as determined by Jahreiss & Wielen (1983) (left panel) and by the Danish group (right panel). Aside from a difference in the age scales used in these studies, the two determinations are broadly consistent with one another. [From data published in Jahreiss & Wielen (1983) and in Strömgren (1987)]

Densidades espaciales (conteo de estrellas)

- 12,000 estrellas con distancias fotométricas (región del PGS)
- dos exponenciales: $\begin{cases} \text{disco delgado } (\sigma_R = 34, \sigma_\phi = 21, \sigma_z = 18 \text{ km/s}) \text{ (} h = 325 \text{ pc)} \\ \text{disco grueso } (\sigma_R = 61, \sigma_\phi = 58, \sigma_z = 39 \text{ km/s}) \text{ (} h = 1.5 \text{ kpc)} \end{cases}$



Gilmore & Reid (1983)

MNRAS 202, 1025

Ojha et al. (1996)

A&A 311, 4560

Figure 10.25 The space density as a function of distance z from the plane of MS stars with absolute magnitudes $4 \leq M_V \leq 5$. The full lines are exponentials with scale heights $z_0 = 300 \text{ pc}$ (at left) and $z_0 = 1350 \text{ pc}$ (at right). The dashed curve shows the sum of these two exponentials. [From data published in Gilmore & Reid (1983)]

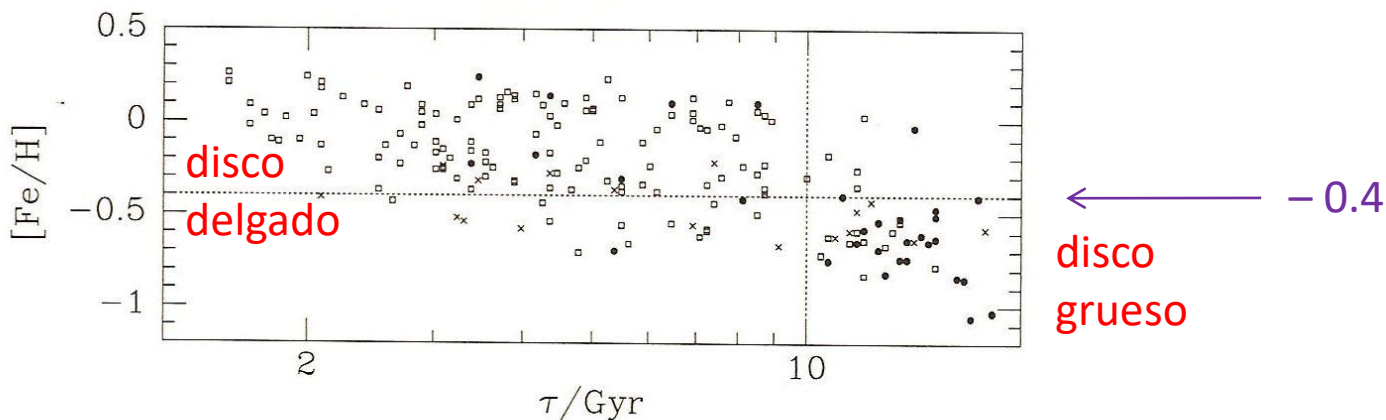


Figure 10.26 A potential division of stars between the thin and thick disks. Stars above and to the left of the dotted lines are assigned to the thin disk, while those below and to the right of the lines are assigned to the thick disk.

Gradientes de metalicidad

- aunque haya mucha dispersión con la edad, la metalicidad de cúmulos abiertos viejos presenta fuerte dependencia con la distancia galactocéntrica.

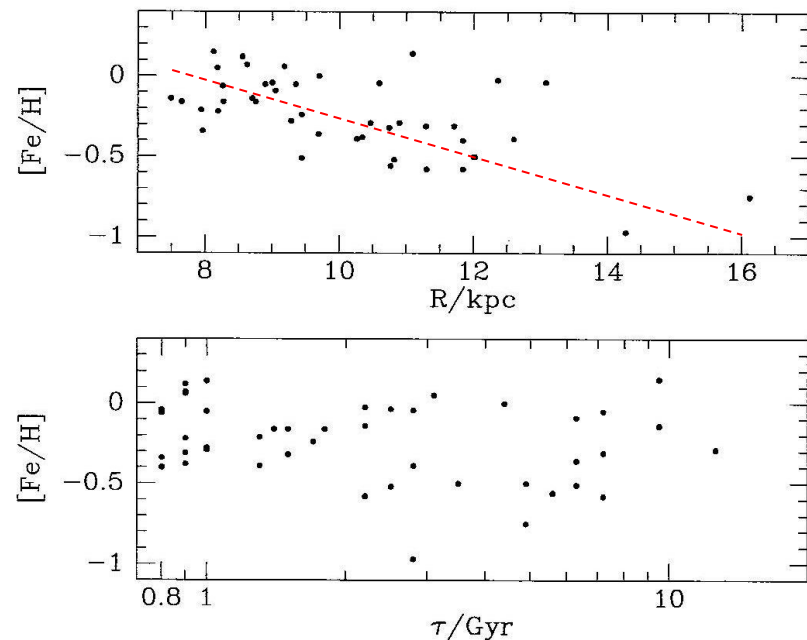


Figure 10.23 The lower panel plots values of $[Fe/H]$ for 44 old disk clusters against estimates of the clusters' ages. The upper panel plots $[Fe/H]$ against the Galactocentric radius of each cluster. [From data published in Friel (1995)]

Disco extremo

- estrellas jóvenes (como las Cefeidas), Cúmulos Abiertos (mas jóvenes que 30 Ma) y regiones HII definen un disco todavía mas delgado, y marcan los brazos espirales de la Galaxia.

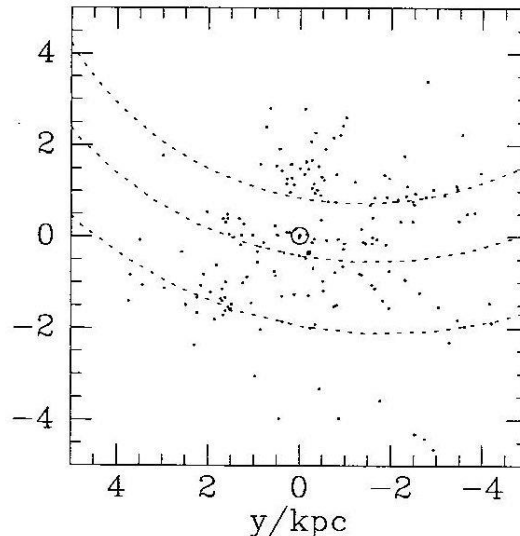
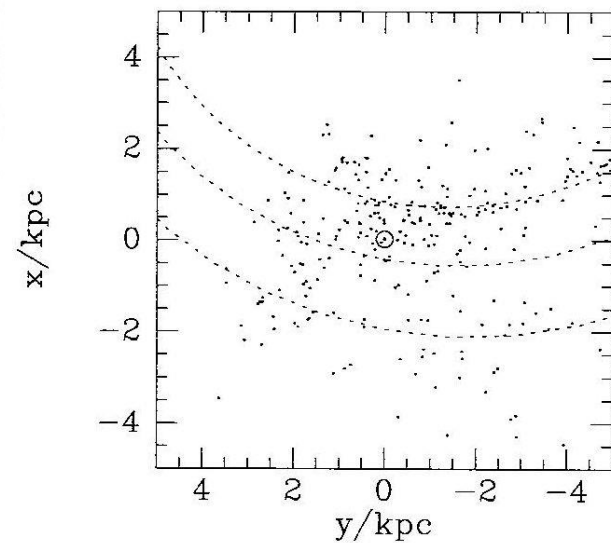
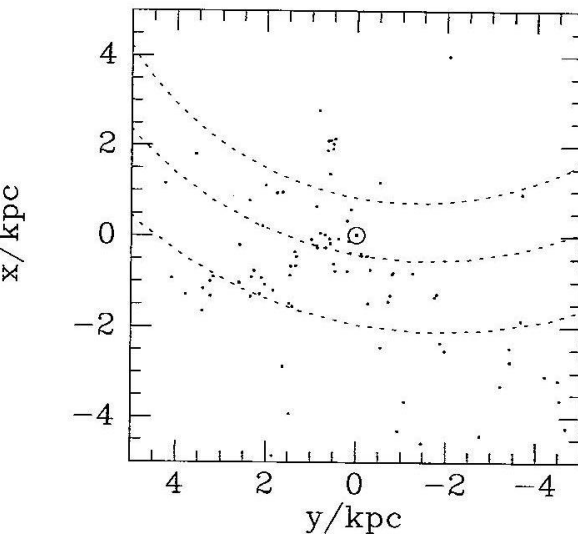
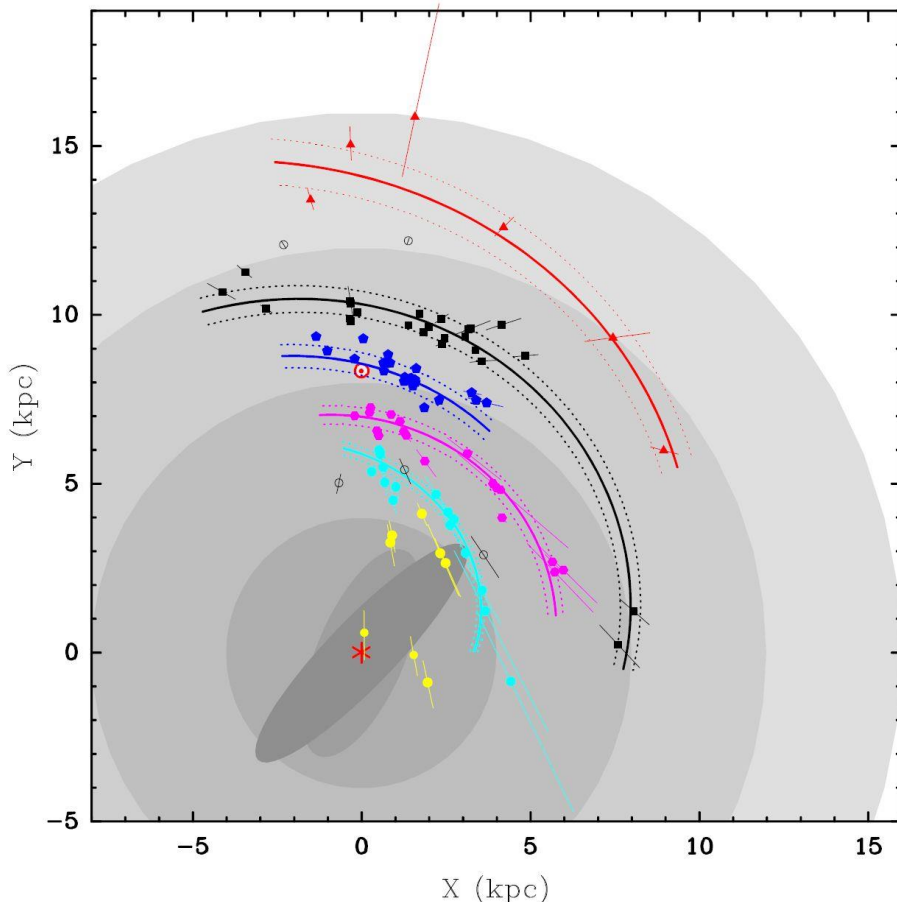


figure 10.28 The distribution of Cepheid variables within 5 kpc of the Sun (left) and of open clusters in Lynga (1987) with ages < 30 Myr (right). The upper two dotted curves in each panel show the ridge-lines of the Sagittarius–Carina arm (top) and the Orion–Cygnus arm (middle) from Figure 9.20.



($h = 130$ pc
 $\varnothing \sim 40$ kpc)

Figure 10.29 Dots mark the locations of 113 HII regions. The Sun, marked by \odot , is at the origin and the direction to the Galactic center is upwards. From top to bottom, dotted curves indicate the ridge-lines of the Sagittarius–Carina, Orion–Cygnus and Perseus arms. [From data published in Blitz, Fich & Stark (1982) and Gillespie *et al.* (1977)]

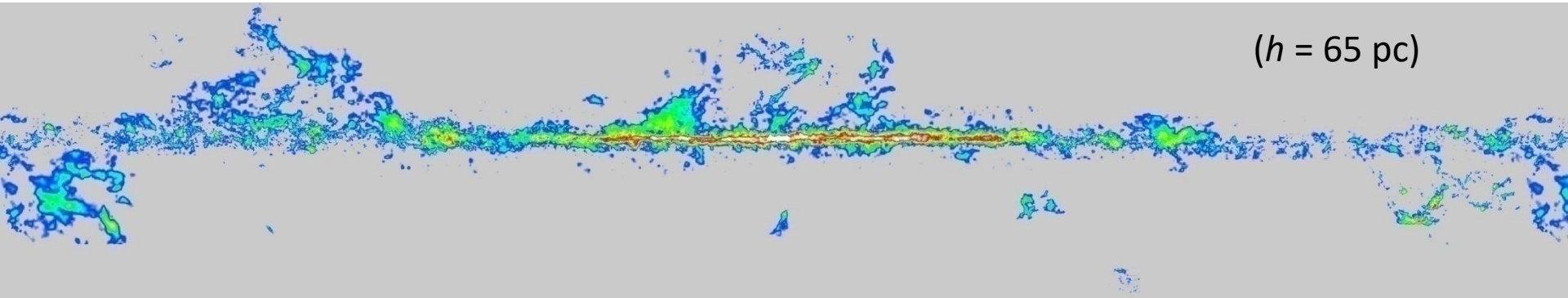


Reid et al. 2014, ApJ 783, A130

Fig. 1.— Plan view of the Milky Way showing the locations of high-mass star forming regions (HMSFRs) with trigonometric parallaxes measured by the VLBA, VERA, and the EVN. The Galactic center (red asterisk) is at (0,0) and the Sun (red Sun symbol) is at (0.8,34). HMSFRs were assigned to spiral arms based primarily on association with structure seen in $\ell - V$ plots of CO and H I emission (and not based on the measured parallaxes): **Inner Galaxy** sources, *yellow dots*; **Scutum arm**, *cyan octagons*; **Sagittarius arm**, *magenta hexagons*; **Local arm**, *blue pentagons*; **Perseus arm**, *black squares*; **Outer arm**, *red triangles*. Open circles indicate sources for which arm assignment was unclear. Distance error bars are indicated, but many are smaller than the symbols. The background grey disks provide scale, with radii corresponding in round numbers to the Galactic bar region (≈ 4 kpc), the solar circle (≈ 8 kpc), co-rotation of the spiral pattern and Galactic orbits (≈ 12 kpc), and the end of major star formation (≈ 16 kpc). The short COBE “boxy-bar” and the “long” bar (Blitz & Spergel 1991; Hammersley et al. 2000; Benjamin 2008) are indicated with shaded ellipses. The *solid* curved lines trace the centers (and *dotted* lines the 1σ widths) of the spiral arms from the log-periodic spiral fitting (see §3 and Table 2). For this view of the Milky Way from the north Galactic pole, Galactic rotation is clockwise.

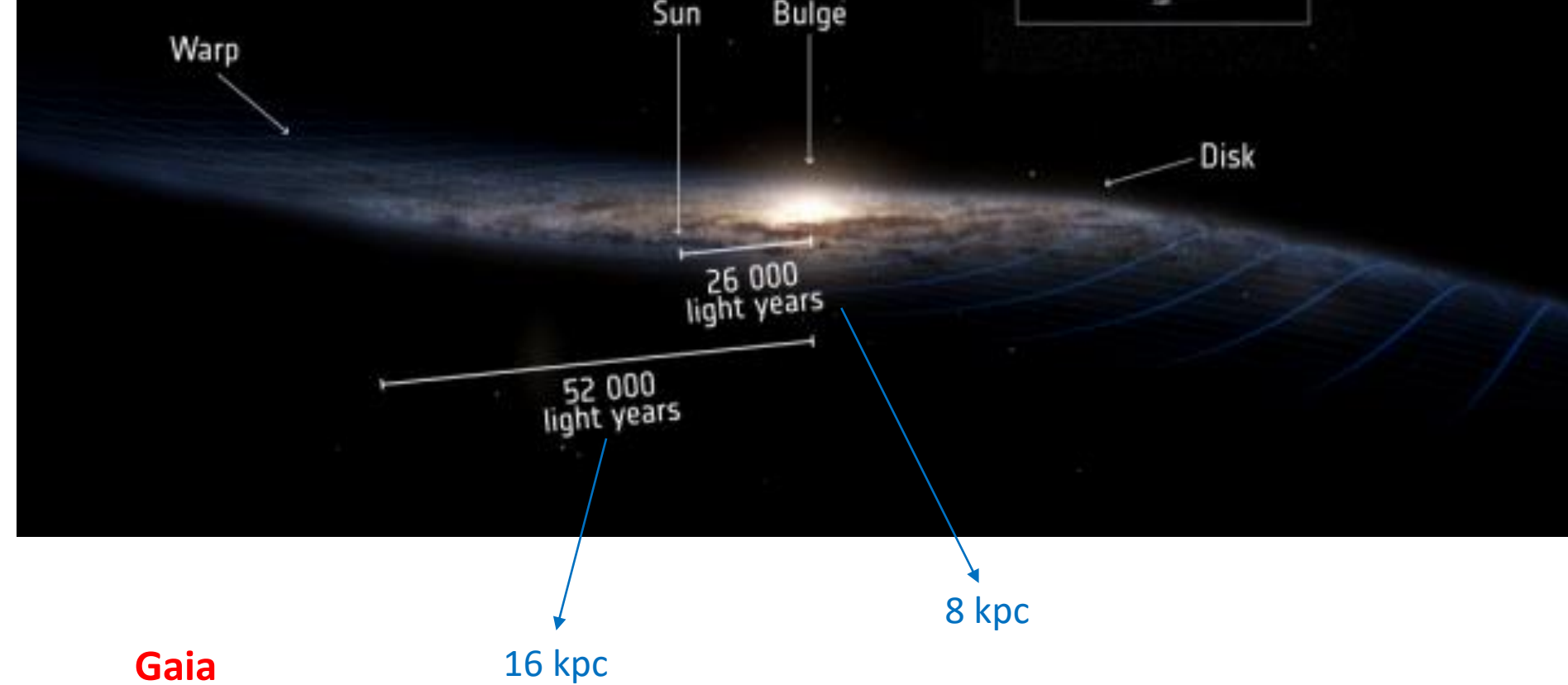
Gas molecular (CO)

- el disco extremo contiene la mayor parte del gas y polvo
- la formación estelar toma lugar en esa región



Radio (CfA 1.2 m, ~2mm)

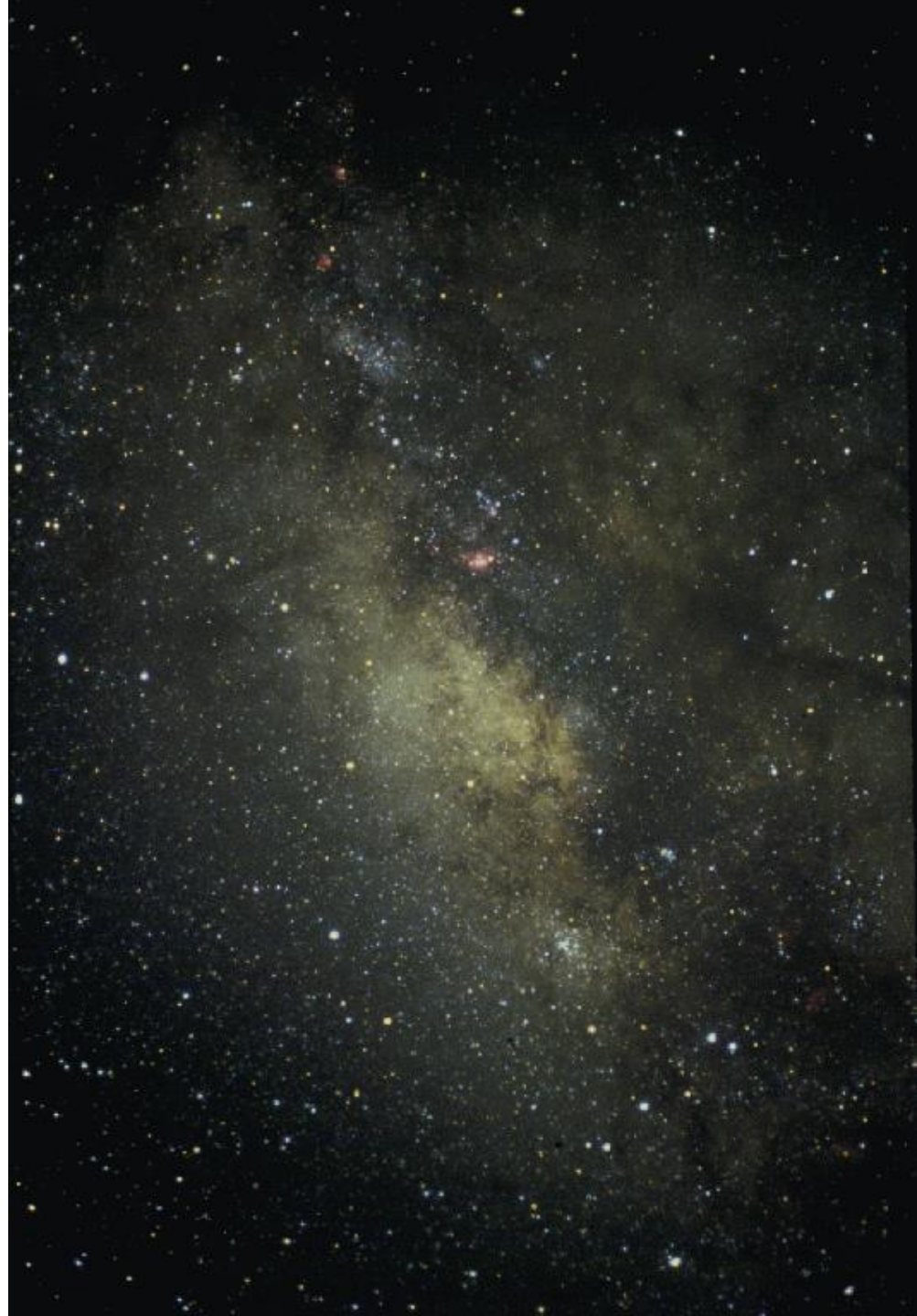
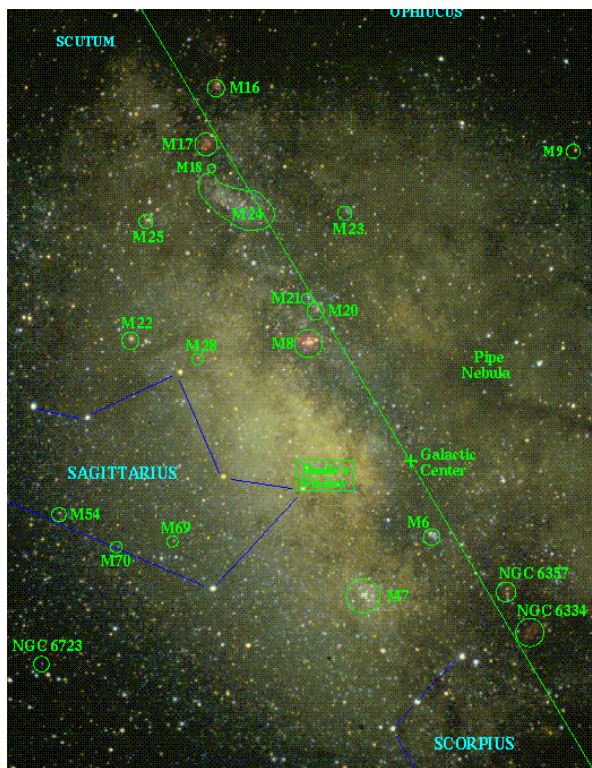
THE MILKY WAY'S WARP



El Bulbo

El bulbo

- componente esferoidal
(perfil de de Vaucouleurs:
 $R_e \sim 0.7 \text{ kpc}$)
- $b/a \sim 0.6$ ($h = 400 \text{ pc}$)
- A_V (centro galáctico) $\sim 28 \text{ mag!}$
- *Ventana de Baade*
($A_V \sim 2 \text{ mag}$, $\ell = 1^\circ$, $b = -4^\circ$)



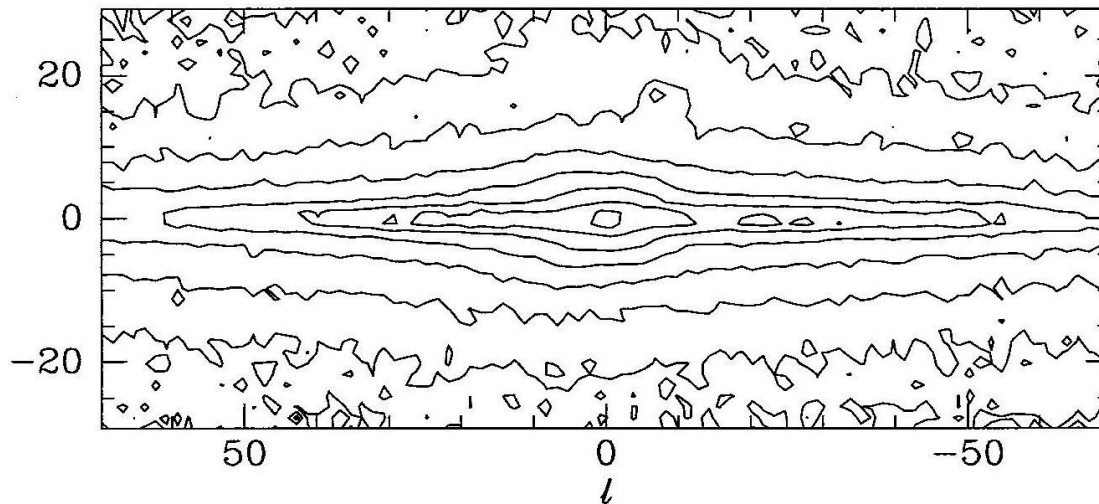
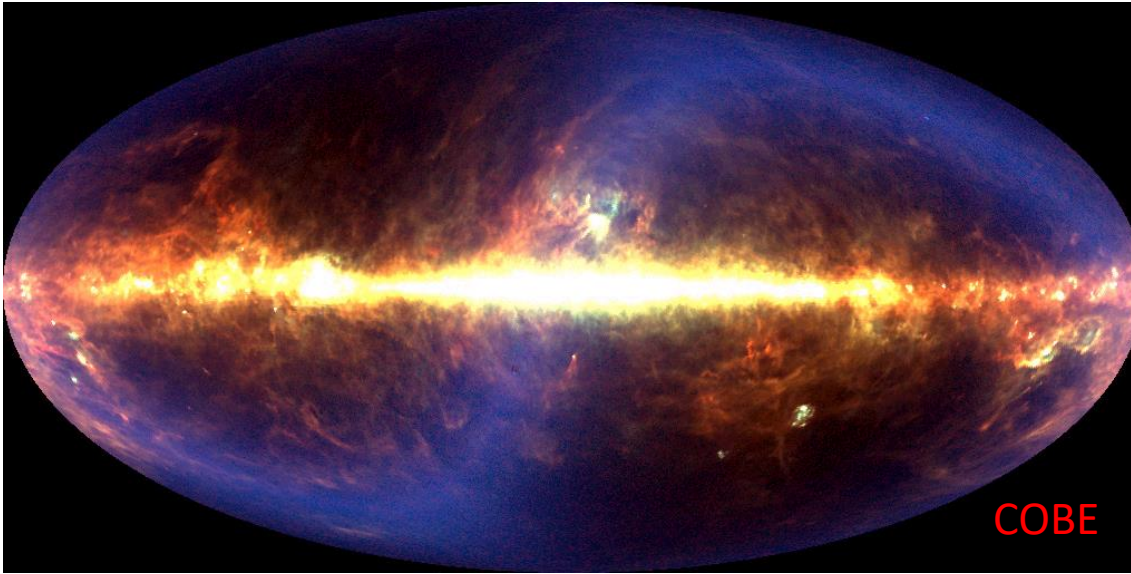


Figure 10.3 A reconstruction of how the Milky Way would appear in the absence of it. The L-band COBE data have been corrected for absorption using equation (10.6) and the dust and stellar luminosity models of Spergel, Malhotra & Blitz (1996). Contours spaced by 1 mag. [After Binney, Gerhard & Spergel (1997)]

La Barra

- método de la resta: $I(l, b) / I(-l, b)$

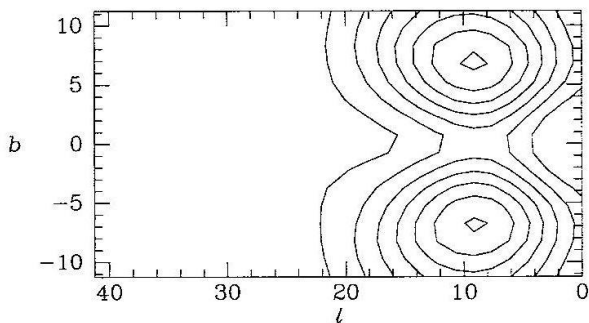
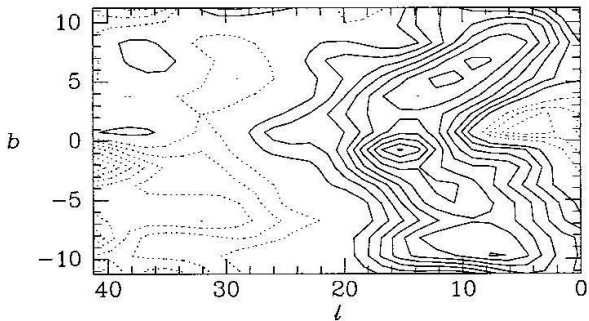


Figure 10.4 The COBE surface photometry displays marked asymmetries in l of the type that would occur if the Galaxy were barred, with the nearer end of the bar at positive l . The top panel shows the ratio $I(l, b) / I(-l, b)$ for the data shown in Figure 10.3. The lower panel shows the prediction of this difference for the bar model that is defined by equation (10.4). The COBE data have been smoothed. Contours are spaced by 0.05 mag. Dotted contours indicate that $I(l, b) < I(-l, b)$.

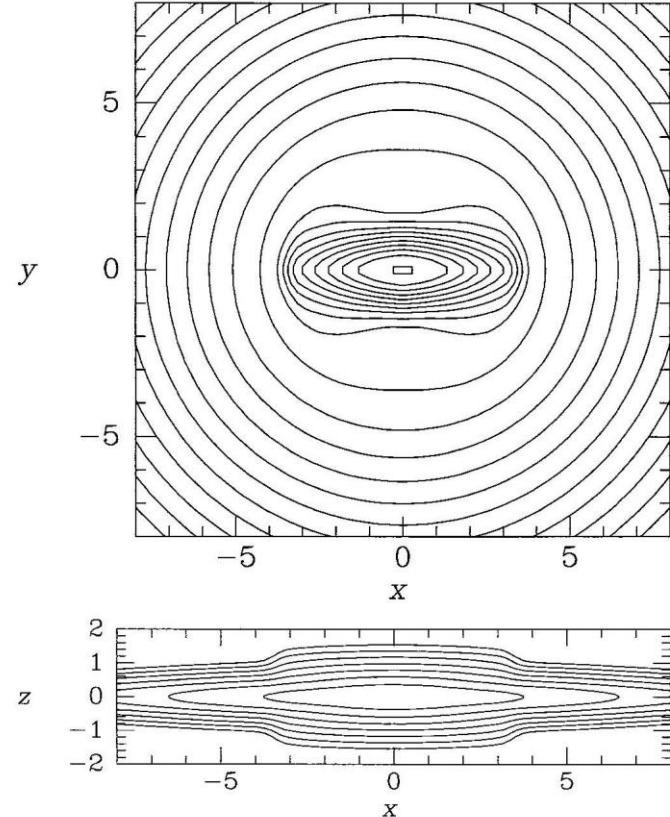
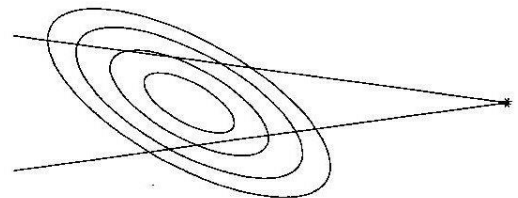
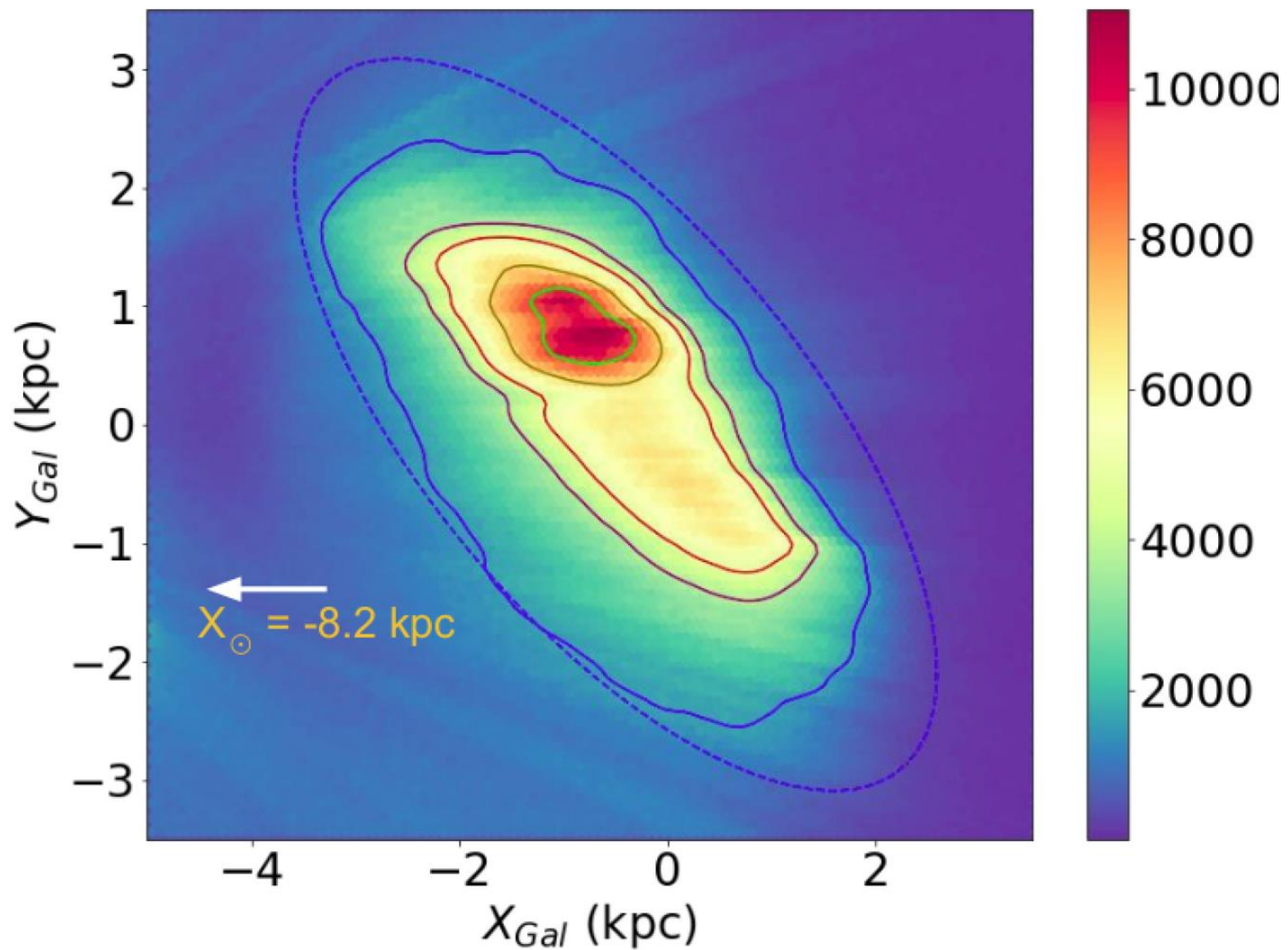
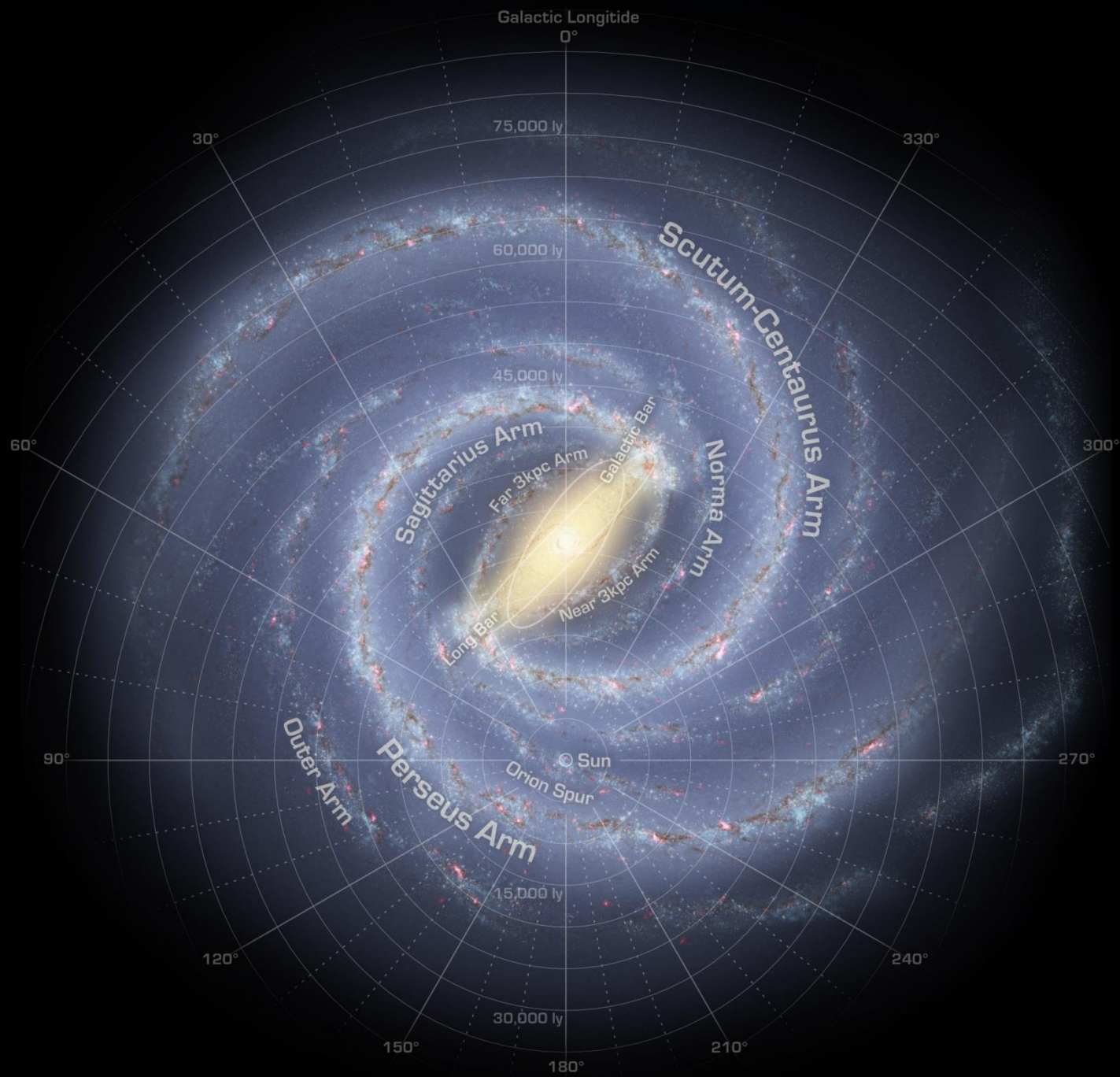


Figure 10.1 Freudreich's model of the inner Galaxy when viewed along the shortest axis of the bar (top) and along to the bar's intermediate axis (bottom). There are ten contours per decade in surface brightness in the upper panel and three per decade in the lower panel. The axes are marked in kpc.

Figure 10.5 The nearer end of a bar generally has higher surface brightness than the further end because for given $|l|$ the left-hand line of sight crosses the long axis of the bar closer to the center than does the right-hand line of sight.

Gaia





Metalicidad y dispersión

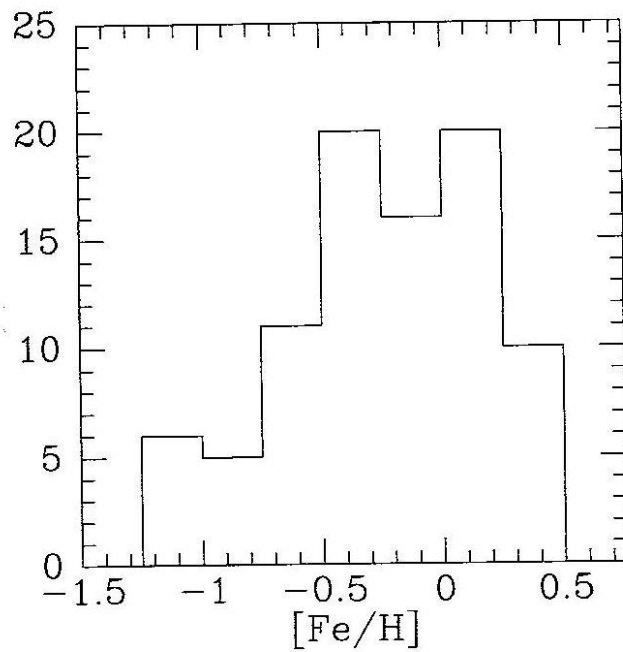


Figure 10.7 The distribution of 88 bulge K giants in $[\text{Fe}/\text{H}]$. [After McWilliam & Rich (1994)]

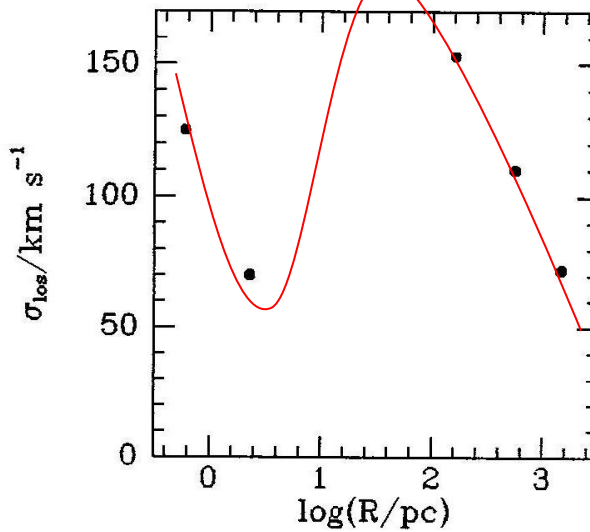


Figure 10.8 Five measurements of the velocity dispersion of stars along lines of sight at $l < 10^\circ$ indicate that the velocity dispersion rises towards the center both within the bulge (outer three points) and within the nuclear star cluster (inner two points), but drops to a minimum between these two dynamically distinct entities.

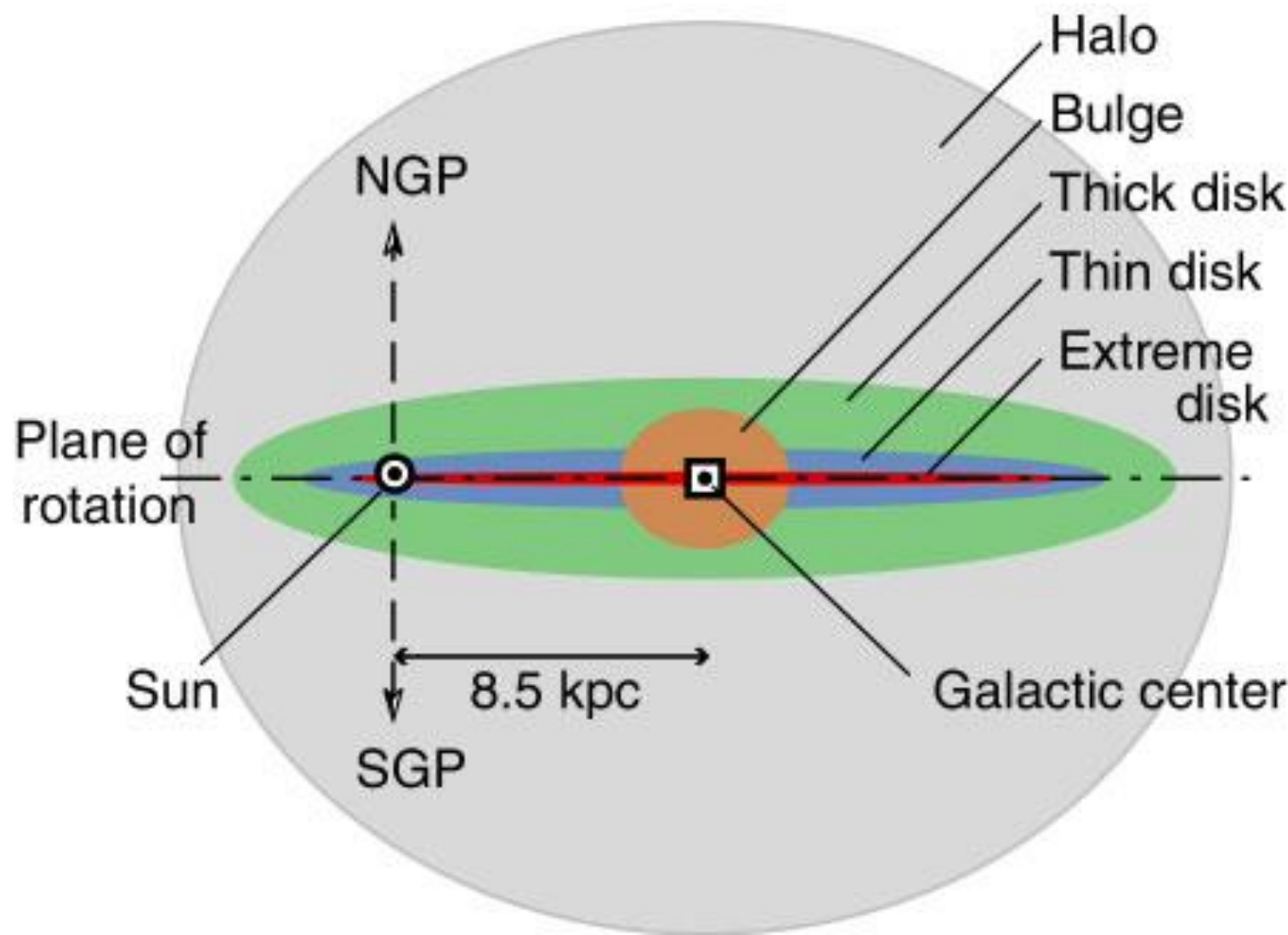


Table 1. Age, metallicity ($[\frac{\text{Fe}}{\text{H}}]$) (mean and dispersion about the mean), radial metallicity gradient (dex/kpc), initial mass function (IMF), and star formation rate (SFR) of the stellar components.

	Age (Gyr)	$[\frac{\text{Fe}}{\text{H}}]$ (dex)	$\frac{d[\text{Fe}/\text{H}]}{dR}$	IMF	SFR
Disc	0–0.15	0.01 ± 0.12	−0.07	$dn/dm \propto m^{-\alpha}$ $\alpha = 1.6$ for $m < 1 M_\odot$ $\alpha = 3.0$ for $m > 1 M_\odot$	constant
	0.15–1	0.03 ± 0.12			
	1–2	0.03 ± 0.10			
	2–3	0.01 ± 0.11			
	3–5	-0.07 ± 0.18			
	5–7	-0.14 ± 0.17			
	7–10	-0.37 ± 0.20			
Thick disc	11	-0.78 ± 0.30	0.00	$dn/dm \propto m^{-0.5}$	one burst
Stellar halo	14	-1.78 ± 0.50	0.00	$dn/dm \propto m^{-0.5}$	one burst
Bulge	10	0.00 ± 0.40	0.00	$dn/dm \propto m^{-2.35}$ for $m > 0.7 M_\odot$	one burst

Table 4. Velocity dispersions ($\sigma_U, \sigma_V, \sigma_W$), asymmetric drift V_{ad} at the solar position (see Sect. 2.1.4) and velocity dispersion gradient $\frac{d\sigma_U}{dR}$.

	Age (Gyr)	σ_U (km s ^{−1})	σ_V (km s ^{−1})	σ_W (km s ^{−1})	V_{ad} (km s ^{−1})	$\frac{d\sigma_U}{dR}$ (km s ^{−1} kpc ^{−1})
Disc	0–0.15	16.7	10.8	6	3.5	-2×10^{-1}
	0.15–1	19.8	12.8	8	3.1	
	1–2	27.2	17.6	10	5.8	
	2–3	30.2	19.5	13.2	7.3	
	3–5	36.7	23.7	15.8	10.8	
	5–7	43.1	27.8	17.4	14.8	
	7–10	43.1	27.8	17.5	14.8	
Thick disc		67	51	42	53	0
Spheroid		131	106	85	226	0
Bulge		113	115	100	79	0

Tarea 4:

El perfil de brillo del bulbo de la Vía-Láctea sigue la ley de $r^{1/4}$ de *Vaucouleurs*, mientras el perfil del disco sigue una ley exponencial. Otro ajuste posible es por el perfil generalizado de *Sérsic*. Describa esos perfiles y como se quedan las distribuciones de brillo del disco y del bulbo en el perfil generalizado de *Sérsic*.